International Summer School
Computational Quantum Materials

My poster in one minute...

Wetting Critical behaviour in a Metal-Mott insulator Interface

A. M. Tagliente, M. Fabrizio

We study a Mott insulator slab in contact with a metallic one away from particle-hole symmetry (Fig 1) by the Gutzwiller approximation, both the conventional one and the so-called ghost-Gutzwiller approximation that gives access to the Hubbard bands and thus to the Kondo proximity effect in the Mott insulator.

The first order nature of the Mott transition away from particle-hole symmetry within the Gutzwiller approximation allows for a wetting critical behaviour characterised by a metal wetting layer that grows logarithmically approaching the first order transition, thus realizing a surface critical phenomenon.
Such critical behaviour shows up both in the electron density and quasiparticle residue.

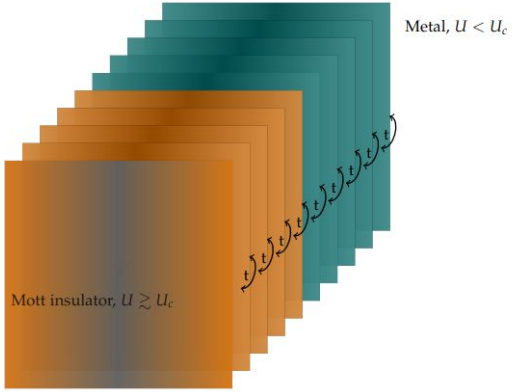

Fig 1: metallic layers coupled to Mott insulating layers by hopping t

Stability of Quantum Spin Liquids in Weak Mott Insulators with a Spin-Orbit Coupling

Asimpunya Mitra, Daniel J. Schultz, Yong Baek Kim

Department of Physics, University of Toronto, Toronto, Ontario M5S 1A7, Canada

arXiv:2404.05806

UNIVERSITY OF TORONTO

Motivation

- Enhanced charge fluctuations in the **weak Mott insulating regime** of the **triangular lattice Hubbard model** gives rise to the **ring-exchange interaction**.
- The ring-exchange interaction can lead to the **chiral spin liquid** (CSL) or a **valence bond solid** (VBS) for some values of t/U.
- How robust are these exotic phases in the presence of a weak spin-orbit coupling (SOC)?

Triangular lattice Hubbard model in presence of a SOC

- Hubbard model on the triangular lattice, with a SOC term breaking inversion.

$$H = \sum_{ij\alpha\beta} \tilde{t}_{ij,\alpha\beta} c^\dagger_{i\alpha} c_{j\beta} + U \sum_i n_{i\uparrow} n_{i\downarrow}, \quad (\mathbf{v}_{ij} = -\mathbf{v}_{ji})$$

$$\tilde{t}_{ij,\alpha\beta} = \begin{cases} t_{ij}\delta_{\alpha\beta} + i\mathbf{v}_{ij}\cdot\boldsymbol{\sigma}_{\alpha\beta} & i,j \text{ nearest neighbours} \\ 0 & \text{otherwise.} \end{cases}$$

- $t_{ij} = t$, and $\mathbf{v}_{ij} = v_z\hat{\mathbf{z}}$. Working in the limit of a weak SOC, ie $|\mathbf{v}|/t < 1$.

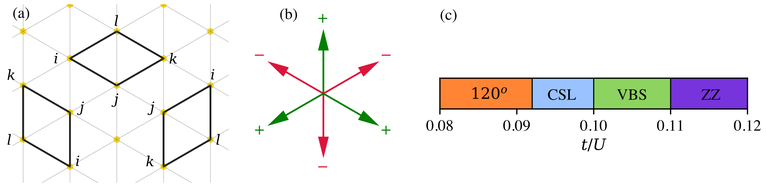

(a) Three types of rings on the triangular lattice $(ijkl)$, (b) sign structure of the $\mathbf{v}_{ij}$, (c) Phase diagram in the absence of a SOC ($\mathbf{v}_{ij} = 0$, $D_z = 0$, $J_{r_1} = 0$) [2].

Simplified spin model and iDMRG specifications

- **Strong-coupling expansion** upto $\mathcal{O}(\tilde{t}^4/U^3)$ to obtain an effective spin model.

$$H_{\text{eff}} = \sum_{\langle ij\rangle} J_1 \mathbf{S}_i\cdot\mathbf{S}_j + \sum_{\langle\langle ij\rangle\rangle} J_2 \mathbf{S}_i\cdot\mathbf{S}_j + \sum_{\langle\langle\langle ij\rangle\rangle\rangle} J_3 \mathbf{S}_i\cdot\mathbf{S}_j + \sum_{\langle ij\rangle} D_z\left(S^x_i S^y_j - S^y_i S^x_j\right) + H_{\text{ring}} + H_{\text{ring,SOC}}.$$

- The **conventional ring-exchange** interaction (without SOC):

$$H_{\text{ring}} = \sum_{(ijkl)\in R} J_r \left((\mathbf{S}_i\cdot\mathbf{S}_j)(\mathbf{S}_k\cdot\mathbf{S}_l) + (\mathbf{S}_j\cdot\mathbf{S}_k)(\mathbf{S}_l\cdot\mathbf{S}_i) - (\mathbf{S}_i\cdot\mathbf{S}_k)(\mathbf{S}_j\cdot\mathbf{S}_l)\right).$$

- SOC-mediated spin bilinear is the **Dzyaloshinskii- Moriya** interaction.
- The leading order **SOC-mediated ring exchange** term:

$$H_{\text{ring,SOC}} = \sum_{(ijkl)\in R} J_{r_1}\Big(S^{[x}_i S^{y]}_j (S^x_k S^x_l + S^y_k S^y_l) + S^{[x}_l S^{y]}_i (S^x_j S^x_k + S^y_j S^y_k) - S^{[x}_j S^{y]}_k (S^x_l S^x_i + S^y_l S^y_i) - S^{[x}_k S^{y]}_l (S^x_i S^x_j + S^y_i S^y_j) + 2S^{[x}_j S^{y]}_l S^z_i S^z_k\Big).$$

- **Treating D_z and J_{r_1} as independent parameters.** J_1, J_2, J_3 and J_r are parametrized in terms of t/U.
- Infinite density matrix renormalization group (**iDMRG**) has been used to find the ground state quantum phase diagram [3].
- We used cylindrical geometry with $L_x = 2$, $L_y = 6$, and bond dimension $\chi = 1600$.

Quantum phase diagrams from iDMRG

Starting from a CSL (VBS) with $\boldsymbol{t/U = 0.097}$ ($\boldsymbol{t/U = 0.105}$) in left (right) subfigure in the absence of a SOC.

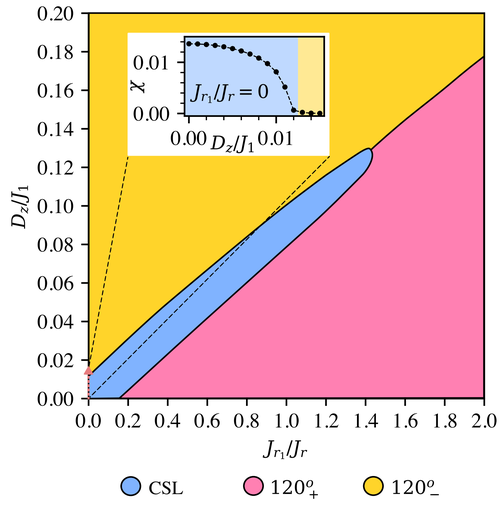

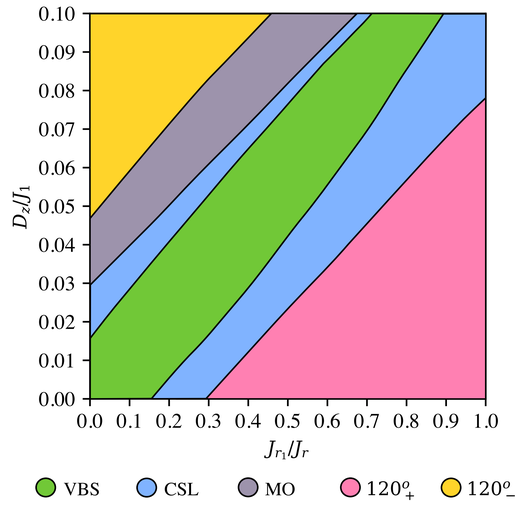

Turning on the SOC stabilizes the CSL (VBS) phase along an elongated narrow region where $\boldsymbol{D_z/J_{r_1} \approx 0.5}$. Stability is a result of compensation between the Dzyaloshinskii-Moriya ($\boldsymbol{D_z}$) interaction and the leading-order SOC-mediated ring-exchange ($\boldsymbol{J_{r_1}}$) interaction.

Quantum phases in presence of SOC

- The 120° (peaked at $S(K)$), CSL ($\chi \neq 0$), VBS (peaked at $D_n(M)$) phases can arise in the absence of a SOC.
- In the CSL phase, entanglement spectrum breaks inversion symmetry and has a characteristic degeneracy pattern [2, 4] of the Kalmeyer-Laughlin state.
- The **SOC** leads to a **non-zero handedness $\boldsymbol{\omega}$**, this is used to sub-classify the 120° ordered phases.
- $\mathbf{120°_+}$ has $\boldsymbol{\omega > 0}$, $\mathbf{120°_-}$ has $\boldsymbol{\omega < 0}$. In absence of SOC, $\mathbf{120°}$ order has $\boldsymbol{\omega = 0}$.
- A new long-ranged **magnetic ordered** (MO) phase with peaks at $S(K)$, correlation length is **shorter** than $120°_\pm$.

$$S(\mathbf{k}) = \sum_{ij}\left(\langle\mathbf{S}_i\cdot\mathbf{S}_j\rangle - \langle\mathbf{S}_i\rangle\cdot\langle\mathbf{S}_j\rangle\right)e^{i\mathbf{k}\cdot(\mathbf{R}_i-\mathbf{R}_j)}, \qquad \chi = \frac{1}{2L_xL_y}\sum_{i,j,k\in\triangleleft,\triangleright}\langle\mathbf{S}_i\cdot(\mathbf{S}_j\times\mathbf{S}_k)\rangle,$$

$$D_n(\mathbf{k}) = \sum_{ij}\left(\langle D^n_i D^n_j\rangle - \langle D^n_i\rangle\langle D^n_j\rangle\right)e^{i\mathbf{k}\cdot(\mathbf{R}_i-\mathbf{R}_j)}, \qquad \omega = \frac{1}{3L_xL_y}\sum_{i,\delta_n}\left\langle S^x_i S^y_{i+\delta_n} - S^y_i S^x_{i+\delta_n}\right\rangle.$$

Heuristic model: Stability of the CSL phase

- In the limit $D_z \gg J_{r_1}$ (in $120°_-$ phase), $H_{\text{eff,A}} = \sum_{\langle i,j\rangle} D_z S^{[x}_i S^{y]}_j$.
  In the limit $J_{r_1} \gg D_z$ (in $120°_+$ phase), $H_{\text{eff,B}} \approx -\frac{1}{2}\sum_{\langle i,j\rangle} J_{r_1} S^{[x}_i S^{y]}_j$, where the four-spin term has been decoupled.
- In the region of stability: $\boldsymbol{H_{\text{eff,A}} + H_{\text{eff,B}} \approx 0 \implies D_z/J_{r_1} \approx 0.5}$ (iDMRG results are within 12%).
- The extent of the CSL can be understood using a **renormalized DM-type interaction**.

$$H_{\text{eff}} = \sum_{\langle i,j\rangle} D_z S^{[x}_i S^{y]}_j \left(1 + \frac{J_{r_1}}{D_z}\sum_{\langle a,b\rangle}\langle S^x_a S^x_b + S^y_a S^y_b\rangle + \frac{2J_{r_1}}{D_z}\sum_{\langle\langle c,d\rangle\rangle}\langle S^z_c S^z_d\rangle\right) \implies \sum_{\langle i,j\rangle}\boldsymbol{\Lambda} D_z S^{[x}_i S^{y]}_j, \tag{1}$$

where $\boldsymbol{\Lambda = 0.1284}$, this nonzero value accounts for the eventual disappearance of the CSL phase. The value of Λ indicates that CSL should be stabilized until $D_z/J_1 \approx 0.097$, this is close to the iDMRG value of $D_z/J_1 = 0.13$.

Heuristic model - continued

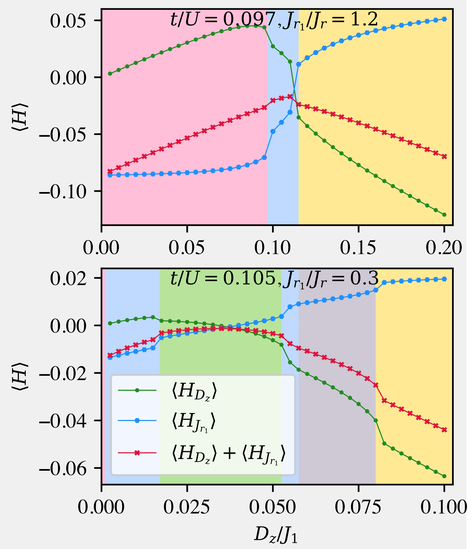

- $\langle H_{D_z} + H_{J_{r_1}}\rangle \approx 0$ in the region where the CSL and VBS phases are stabilized.

Conclusions

- The **CSL** and **VBS** phases of the triangular lattice Hubbard model can be **stabilized in the presence of a weak SOC**.
- The stabilization is a result of **compensation** between two types of SOC-mediated spin interactions: the **Dzyaloshinskii- Moriya** interaction and the leading order **SOC-mediated ring-exchange** interaction.
- Essential features of the compensation mechanism captured by our heuristic model, including the ratio of $D_z/J_{r_1} \approx 0.5$ for compensation, and extent of the CSL phase.

References

[1] *arXiv:2404.05806, cond-mat.str-el*, 2024.

[2] *arXiv:2309.00037, cond-mat.str-el*, 2023.

[3] *SciPost Phys. Lect. Notes*, page 5, 2018.

[4] *Phys. Rev. Lett.*, 127:087201, Aug 2021.

NSERC CRSNG

Physics UNIVERSITY OF TORONTO
Centre for Quantum Materials

Orbital Competition in Bilayer Graphene's Fractional Quantum Hall Effect

Bishoy Kousa, The University of Texas at Austin

- Bernal Bilayer graphene in a magnetic field:
  - Large even denominator gaps measured
  - Nearly degenerate $n = 0, n = 1$ Landau Levels
- Exchange interactions with the negative energy sea lifts this degeneracy and compete with single particle splitting
- Where do we get pure $n = 1$ correlations

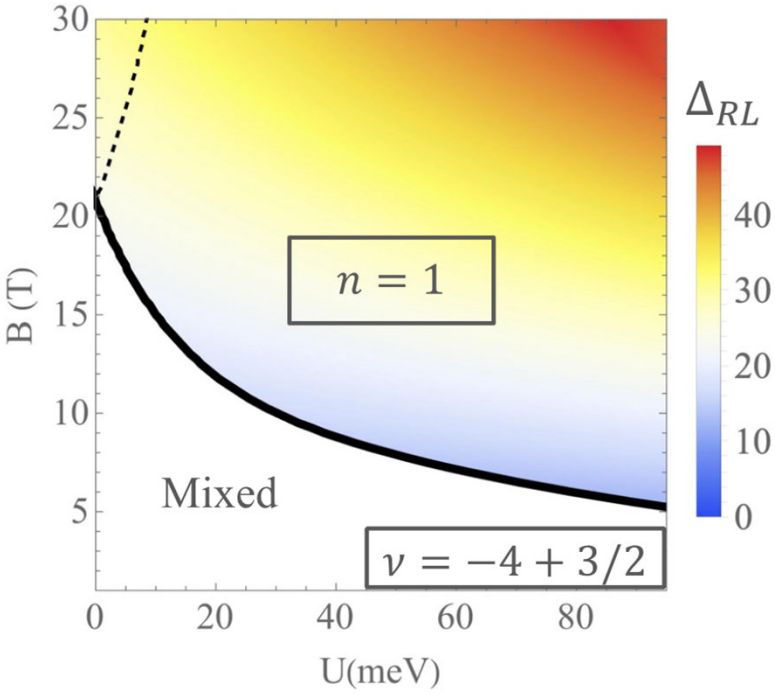

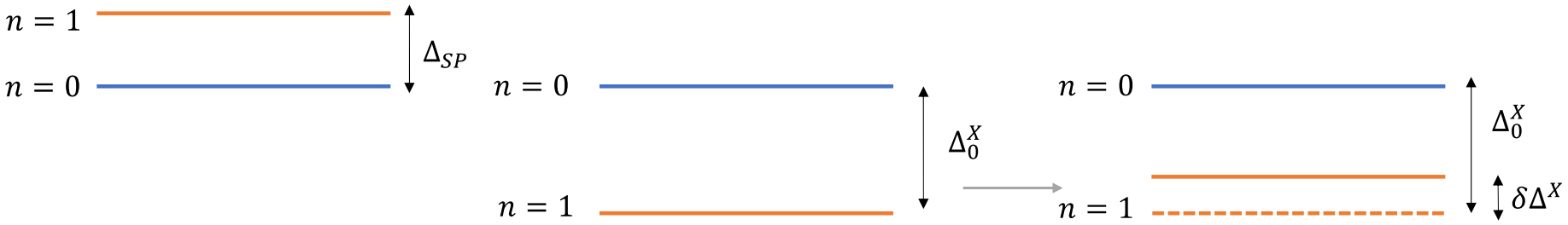

arXiv:2402.10440

An Improved Two-Particle Self-Consistent Approach

C. Lahaie, C. Gauvin-Ndiaye, Y.M. Vilk, A-M. S. Tremblay

One of the Important models for the study of cuprates is the 2D Hubbard model

$$H = -\sum_{\langle i,j\rangle\sigma} t_{ij}(c^{\dagger}_{i\sigma}c_{j\sigma} + c^{\dagger}_{j\sigma}c_{i\sigma}) + U\sum_{i} n_{i\uparrow}n_{i\downarrow}$$

- **TPSC** is an approach to solve the 2D Hubbard model
- **TPSC** has been used to study the **antiferromagnetic pseudogap** (T*) as it reproduces **ARPES measurements** in electron-doped cuprates.
- However, **TPSC** is **NOT** valid deep below the **T* line**.

Thus, we propose an improvement to the **TPSC** approach called **TPSC+** to solve this problem

Experimental electron-doped cuprates phase-diagram of $Nd_{2-x}Ce_xCuO_{4-y}$

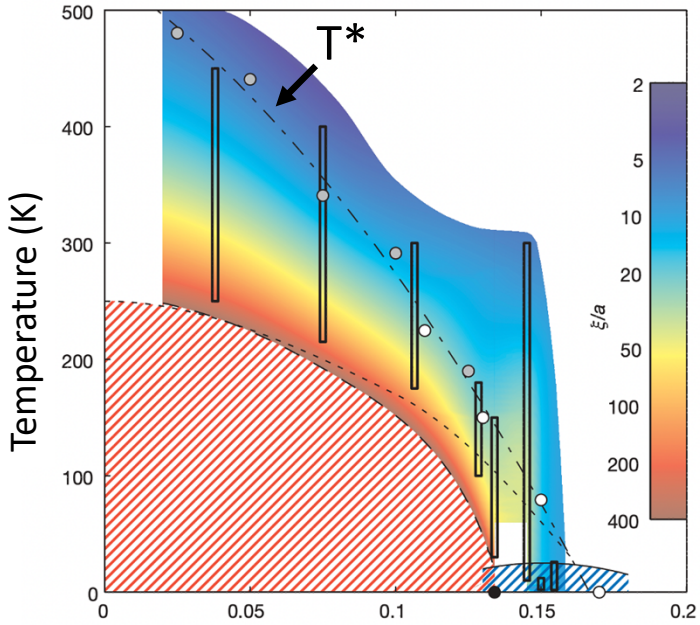

Motoyama, *Nature 445*, nº 7124 :186-89.

Wavelet-Representation of Two-Particle Correlation Functions and Diagrammatic Equations

E. Moghadas, N. Dräger, A. Toschi, J. Zang, M. Medvidović, D. Kiese, A. Millis, A. Sengupta, S. Andergassen, D. Di Sante

- Wavelet-Transform: $W_\psi(j,x) = \int_{-\infty}^{\infty} dt\, f(t)\, \frac{1}{\sqrt{j}} \psi^*\left(\frac{t-x}{j}\right)$

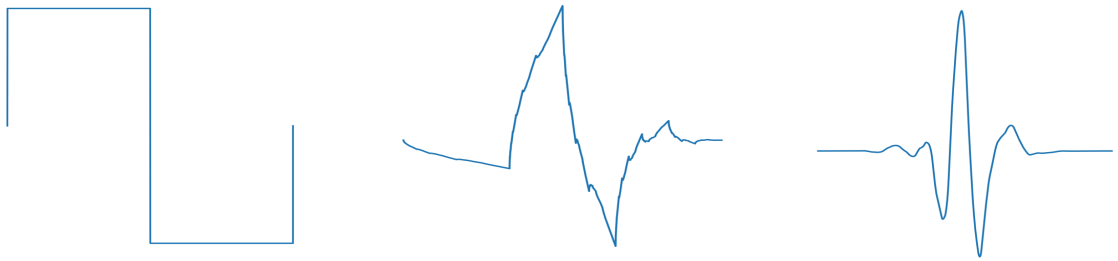

- Compact representation of **Two-Particle Quantities**

$$\chi^{\nu\nu'} = \sum_{x,y} W_\phi\,(j_0,x,y)\phi^{\nu\nu'}_{j_0xy} + \sum_{j,x,y} W_\psi\,(j,x,y)\psi^{\nu\nu'}_{jxy}$$

- **Diagrammatic Equations** in Wavelet Basis

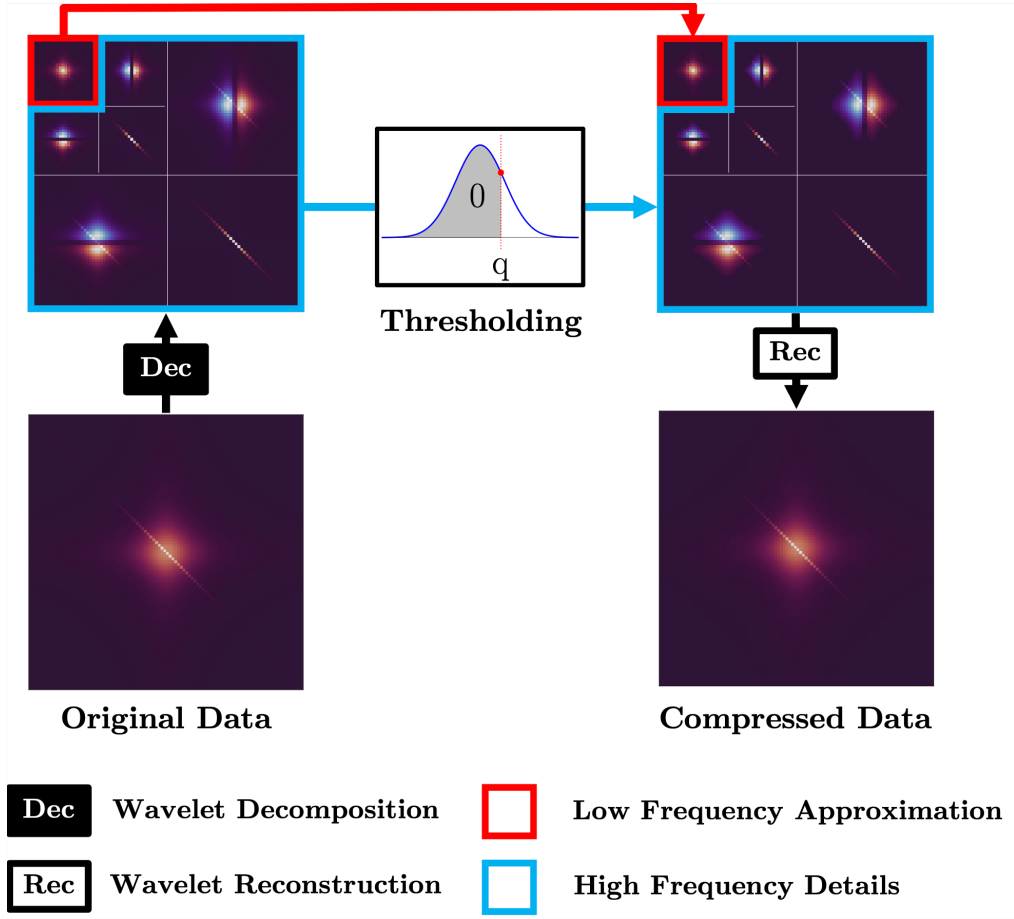

E. Moghadas, N. Dräger *et al.*, arXiv:2402.13030, 2024

Nickelate and cuprate superconductors

Nickelates

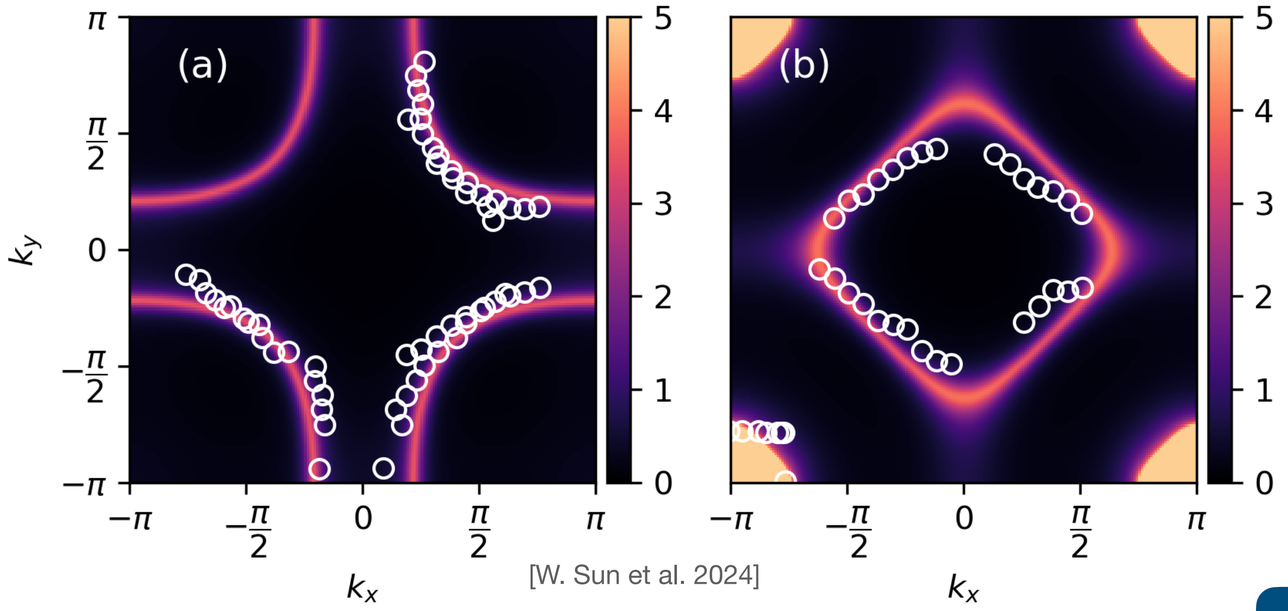

[W. Sun et al. 2024]

[M. Kitatani et al. 2020]

Cuprates

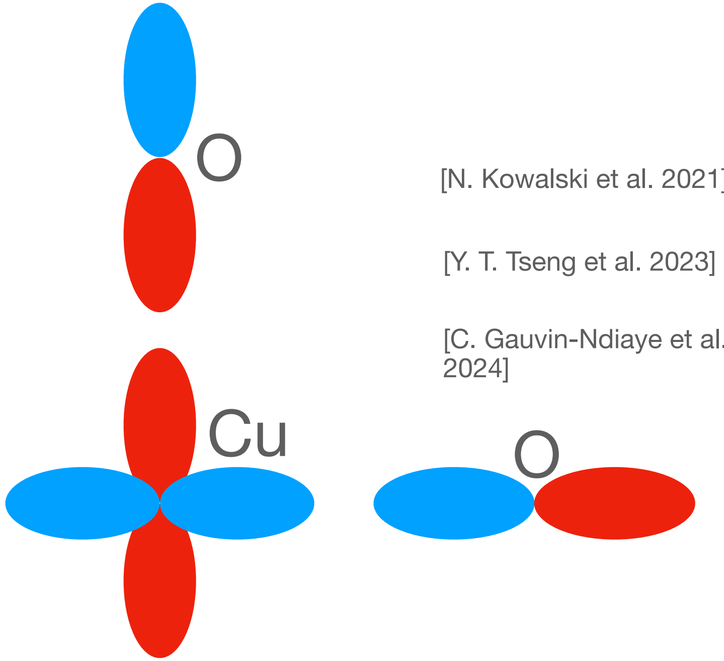

[N. Kowalski et al. 2021]

[Y. T. Tseng et al. 2023]

[C. Gauvin-Ndiaye et al. 2024]

Eric Jacob
Computational Quantum Materials School
May 2024

TU WIEN TECHNISCHE UNIVERSITÄT WIEN

Q-M&S. Correlated Quantum Materials & Solid State Quantum Systems

Relativistic corrections to LO-TO Splitting

The Phonon Polariton is a hybrid mode: we want to derive the weight of the two components

$$S = S_{\mathrm{Ph}} + S_{\mathrm{EM}} + S_{\mathrm{MC}}$$

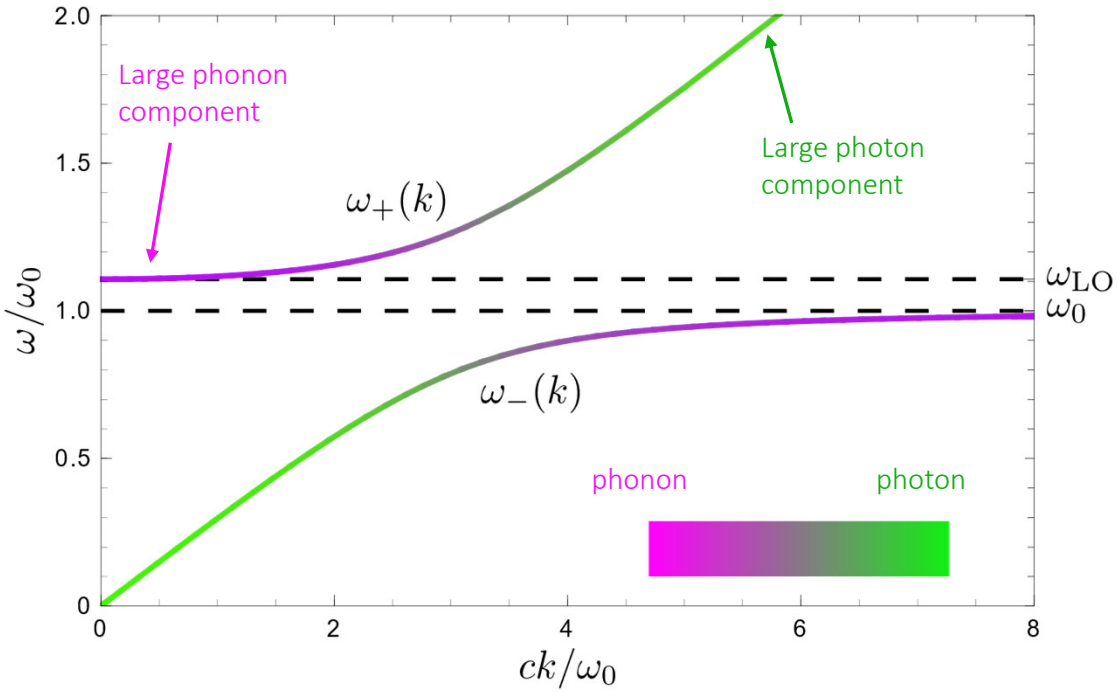

Entanglement in the Hubbard Model

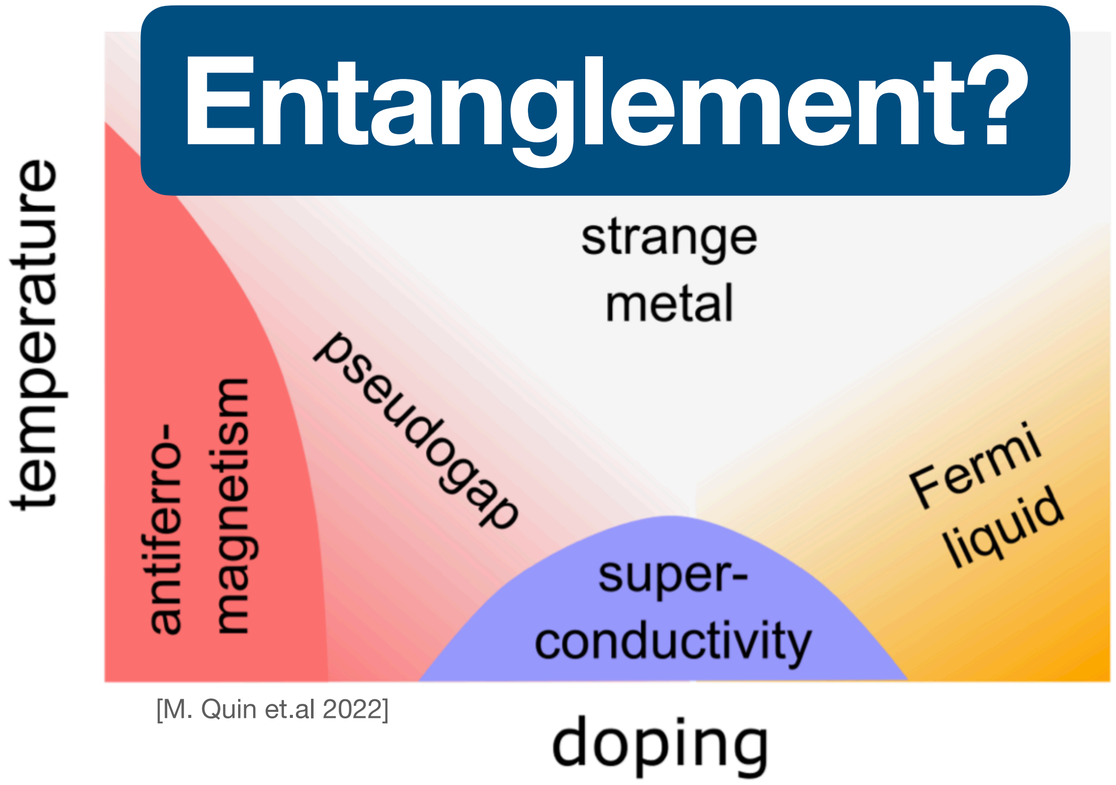

[M. Quin et.al 2022]

- Two-site reduced density matrix from $G^{(2)}, G^{(4)}$
  - Negativity
  - Mutual Information
- Results for small clusters

[G. Roosz, A. Kauch, **FB**, Karsten Held 2023]

Frederic Bippus
Computational Quantum Materials School
May 2024

TU WIEN TECHNISCHE UNIVERSITÄT WIEN

Q-M&S. Correlated Quantum Materials & Solid State Quantum Systems

Phases and Phase Transition in Disordered q-state Clock Model

Gaurav Khairnar[1], Vishnu PK[2], Rajesh Narayanan[2], Thomas Vojta[1]
[1]Missouri University of Science and Technology, Rolla, USA
[2] Indian Institute of Technology, Madras, India

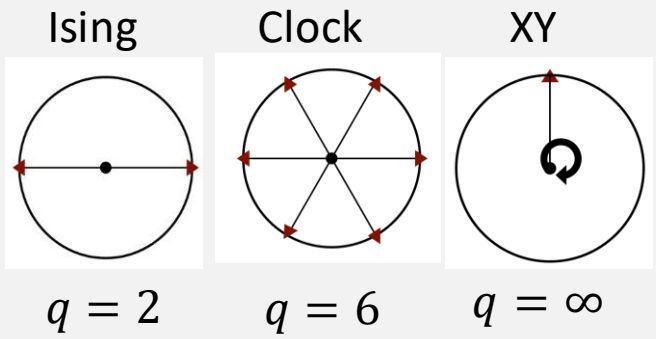

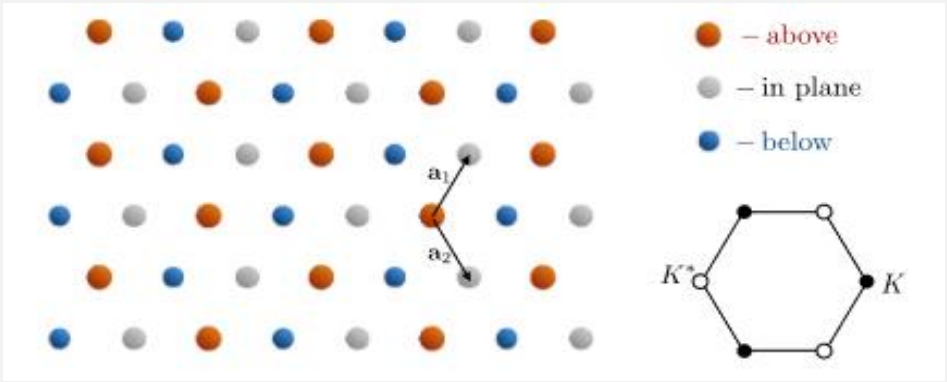

e.g. Buckling Transition

Highlights:

- Multiple phases and phase transitions
- Strong disorder renormalization group theory predictions
- Expected multi-critical point
- Weak to strong disorder crossover

Phase Diagram:

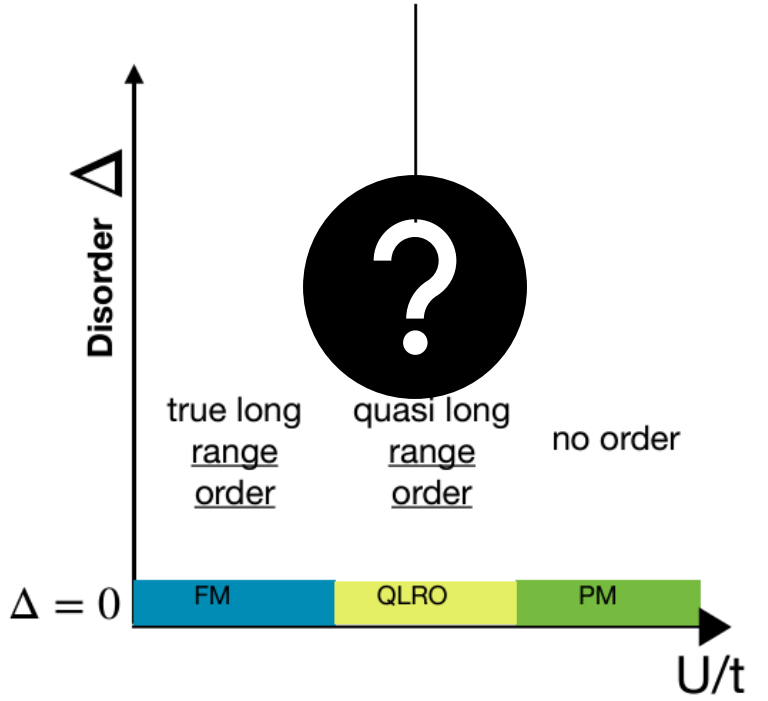

Momentum and finite doping effects in a Metal-Mott insulator interface

- We investigate the interface between a Mott insulator and a metal away from half filling using single site DMFT and DCA
- In this kind of interface there is penetration of metallicity in the Mott insulator characterised by a surface layer that develops a finite quasiparticle effect, known as Kondo proximity effect. We study how this phenomenon modifies the density profile in the Mott insulator when the chemical potential is away from the particle-hole symmetric point.
- In DCA, a cluster extension of DFMT, a momentum differentiation of the Mott transition occurs. We are interested in the interplay of this physics with the aforementioned proximity effect, in particular in the evolution of the Fermi surface inside the Mott insulator as well as the possible occurrence of a pseudogap or Fermi pockets

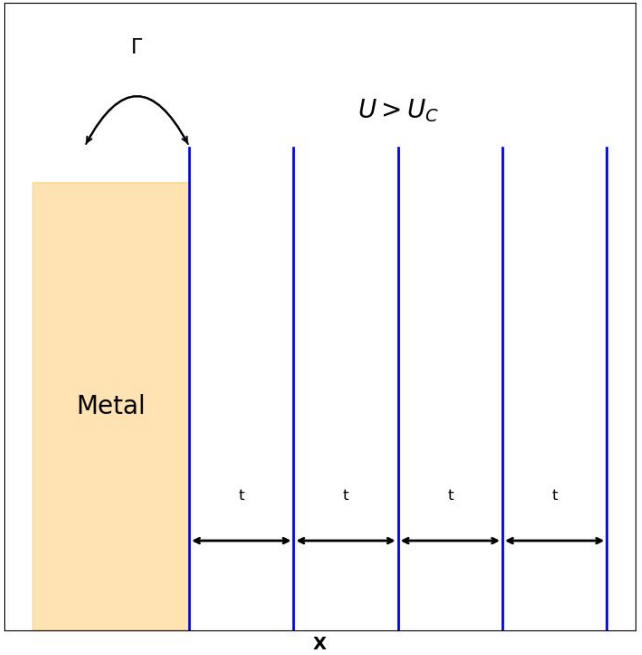

Gregorio Staffieri, Michele Fabrizio

Order by Quantum Disorder in the Heisenberg-Compass Model on the Square Lattice: A Perspective from Exact Diagonalization

Subhankar Khatua[1,2], **Griffin C. Howson**[1], Michel J. P. Gingras[2], Jeffrey G. Rau[1]

[1] *Department of Physics, University of Windsor, Windsor, Ontario, Canada*

[2] *Department of Physics and Astronomy, University of Waterloo, Waterloo, Ontario, Canada*

Motivating Question

What are the signatures of order by disorder in the Heisenberg-compass model on small square clusters?

The Heisenberg-Compass Model

- Bond–dependent magnetic interactions have been explored for generating new phases of matter [1]
  - Typically found in transition metal oxides [2,3]
  - Leads to competing interactions which can not be simultaneously satisfied – a phenomenon known as *frustration*
- A simple, yet intriguing bond-dependent model is the Heisenberg-compass model on the square lattice

$$\mathcal{H} = \sum_{\langle ij \rangle_\gamma} J \boldsymbol{S}_i \cdot \boldsymbol{S}_j + K S_i^\gamma S_j^\gamma$$

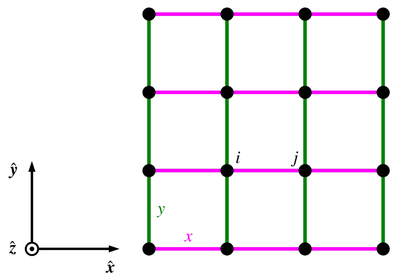

FIG. 1: Heisenberg-compass model on a square lattice with bond definitions.

- Set $J = \cos\xi$ and $K = \sin\xi$, which fixes the energy scale to units of $\sqrt{J^2 + K^2} = 1$
  - Classically, there are six regimes in the range of $\xi \in [0, 2\pi)$ exhibiting distinct ground states

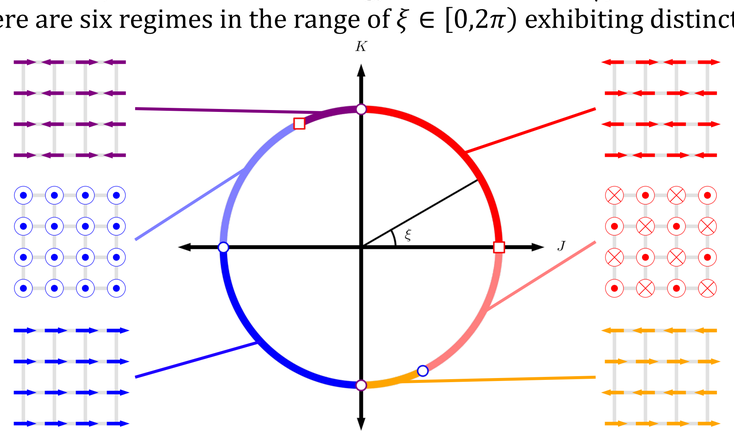

FIG. 2: Classical phase diagram of the Heisenberg-compass model over the full range of ξ.

- The in-plane ground states can be rotated in-plane without any cost in energy – U(1) degeneracy
  - Not a symmetry of the compass term!
    - Only discrete C_4 rotation about the $\hat{\boldsymbol{z}}$ axis and discrete C_2 rotations about the $\hat{\boldsymbol{x}}$ and $\hat{\boldsymbol{y}}$ axes
  - Introduce quantum fluctuations to select for ground states that are related by these symmetries of the Hamiltonian – a phenomenon known as *order by disorder* [4].

Order by Disorder (ObD)

- Fluctuations tend to suppress order, but this is not always the case
  - A model may permit some *accidental classical degeneracy* which is not protected by the symmetry of the Hamiltonian
  - Fluctuations (e.g. quantum or thermal [5]) can generate an energy gap between the true symmetry protected degenerate ground states and nearby excited states

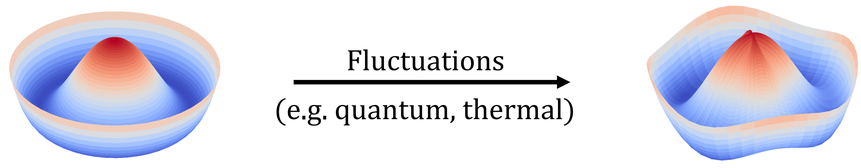

FIG. 3: A schematic illustration of order by disorder.

Method

- Solve the Hamiltonian by exact diagonalization (ED) [6]
  - Provides exact ground state properties for small clusters
  - Hilbert space scales as 2^N for a system of N $S = 1/2$ spins
    - Discrete translation symmetry → work in momentum space!
      - N allowed translations → N blocks of roughly size $2^N/N$
      - Blocks can be diagonalized separately using Lanczos methods [7]

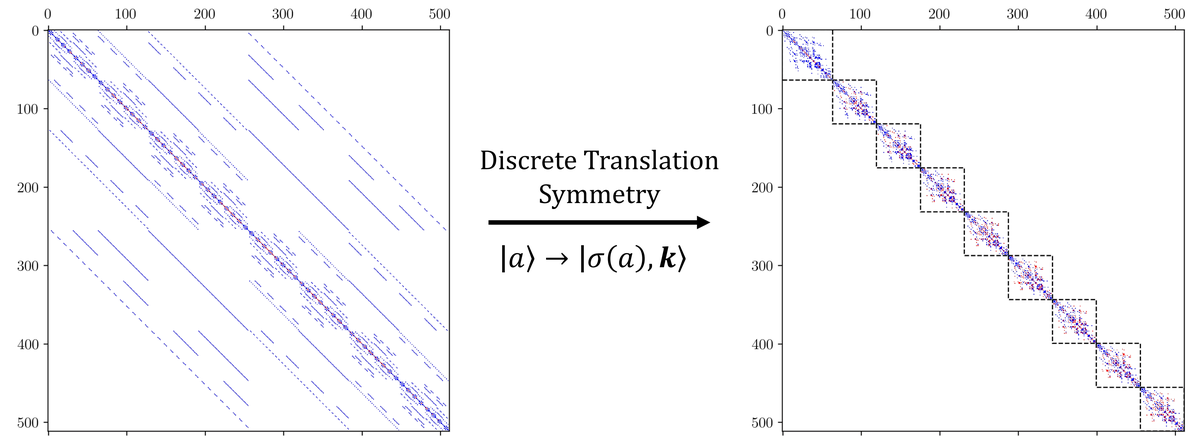

FIG. 4: Effect of block-diagonalization procedure for L = 3 at $\xi = \pi$ (ferromagnet)

Results

Ground State Energy

- Using ED, obtain the ground state energy eigenvalue E_0 and eigenvector for all values of ξ
  - Phase boundaries are identified by peaks in $-\frac{\partial^2 \varepsilon_0}{\partial \xi^2}$
    - Strong qualitative agreement with classical phase boundaries – no evidence of ObD

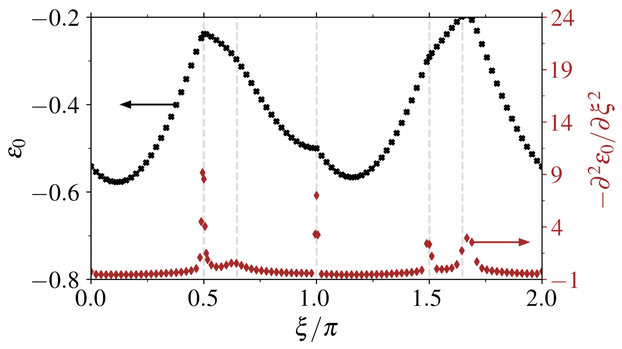

FIG. 5: Ground state energy density, ε_0, and the second derivative of ε_0 with respect to ξ for L = 4. The second derivative spikes at the classical phase boundaries (grey dashed lines).

Phase Diagram

- The static structure factor, $\mathcal{S}(\boldsymbol{Q})$, reveals the magnetic ordering of the ground state

$$\mathcal{S}_{\mu\mu}(\boldsymbol{Q}) = \frac{1}{N} \sum_{i,j} e^{-i\boldsymbol{Q}\cdot(\boldsymbol{r}_i - \boldsymbol{r}_j)} \left\langle S_i^\mu S_j^\mu \right\rangle$$

where $\mu = x, y, z$ and $\langle \cdots \rangle$ denotes an expectation value in the ground state

- Compute at four high symmetry points in the Brioullin zone
  - $\boldsymbol{\Gamma} = \boldsymbol{0}, \boldsymbol{X} = (\pi, 0), \boldsymbol{Y} = (0, \pi)$ and $\boldsymbol{M} = (\pi, \pi)$
- Strong qualitative agreement with classical phase diagram – no evidence of ObD

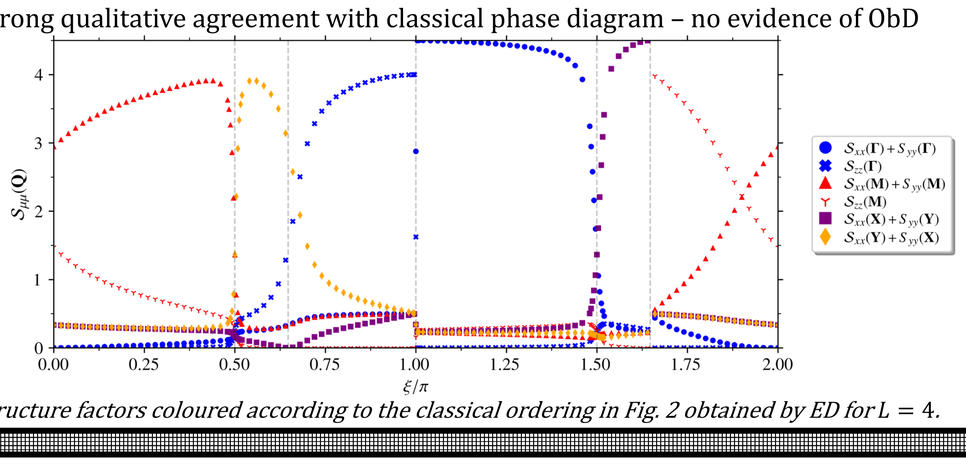

FIG. 6: Structure factors coloured according to the classical ordering in Fig. 2 obtained by ED for L = 4.

Observation of Order by Disorder

- Identify two potential signatures of order by disorder:
  1. Energy gap
     - The energy gap, $E - E_0$, is presented in Fig. 7
       - For comparison, semiclassical results are depicted, as well
       - The gap from these three methods exhibit strong agreement in the out-of-plane phases
         - This is *not* where ObD occurs – some other diagnosis is needed!

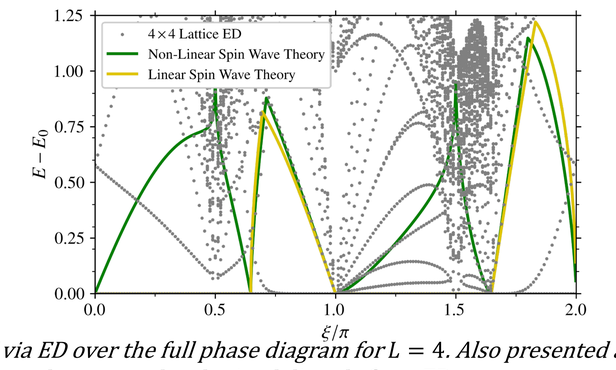

FIG. 7: Energy gap obtained via ED over the full phase diagram for L = 4. Also presented are results of semiclassical methods, which suggest where the gap can be obtained directly from ED.

  2. In-plane magnetization
     - Introduce small field to in-plane antiferro- (AFM) and ferromagnetic (FM) phases, $-\sum_i \boldsymbol{h}_i \cdot \boldsymbol{S}_i$
       - FM: Field is added uniformly, $\boldsymbol{h}_i = h(\cos\phi\, \hat{\boldsymbol{x}} + \sin\phi\, \hat{\boldsymbol{y}})$
       - AFM: Field is staggered, $\boldsymbol{h}_i = (-1)^i h(\cos\phi\, \hat{\boldsymbol{x}} + \sin\phi\, \hat{\boldsymbol{y}})$
- Without ObD, model will fully polarize along $\hat{\boldsymbol{h}}$, independent of ϕ
  - Quantum mechanically, states polarize more strongly along $\phi = 0, \frac{\pi}{2}$ $\left(\pi, \frac{3\pi}{2}\right.$ by $\left.C_4\right)$

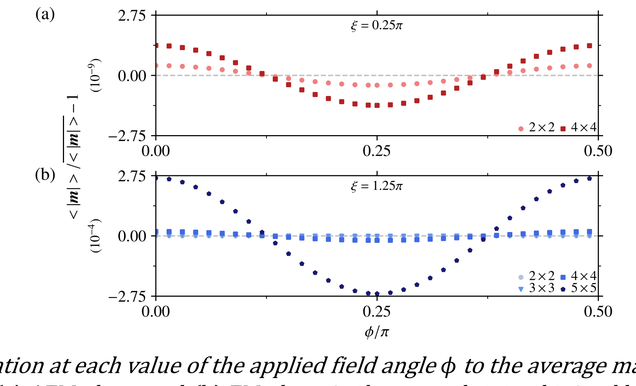

FIG. 8: Ratio of magnetization at each value of the applied field angle ϕ to the average magnetization over the full range of ϕ for $h = 10^{-4}$ in the (a) AFM phase and (b) FM phase in the ground state obtained by ED for various system sizes.

Conclusion

- ED reveals a phase diagram that is qualitatively similar to the classical phase diagram
- The energy gap can be read directly from some regions of the phase diagram, but not where ObD needs to be diagnosed
- The in-plane magnetization under a perturbing field reveals that the system favours states that point along the $\pm\hat{\boldsymbol{x}}, \pm\hat{\boldsymbol{y}}$ axes, suggesting that these are the symmetry protected ground states of the model

References

[1] Z. Nussinov and J. ver den Berk, "Compass models: Theory and physical motivations," Rev. Mod. Phys. **87**, 1-59 (2019)

[2] K. I. Kugel and D. I. Khomskii, "The Jahn-Taller effect and magnetism: transition metal compounds," Sov. Phys. Usp. **24**, 231-256 (1982)

[3] G. Jackeli and G. Khaluillin, "Mott Insulators in the Strong Spin-Orbit Coupling Limit: From Heisenberg to a Quantum Compass and Kitaev Model," Phys. Rev. Lett. **102**, 017205 (2009)

[4] J. Villain, R. Bidaux, J.-P. Carton and R. Conte, "Order as an Effect of Disorder," J. Phys. France **41** 1263-1272 (1980)

[5] S. Khatua, M. J. P. Gingras and J. G. Rau, "Pseudo-Goldstone Modes and Dynamical Gap Generation from Order by Thermal Disorder," Phys. Rev. Lett. **130**, 266702 (2023)

[6] A. W. Sandvik, "Computational Studies of Quantum Spin Systems," AIP Conference Proceedings **1297**, 135-338 (2010)

[7] K. Wu and H. Simon, "Thick-restart Lanczos method for large symmetric eigenvalue problems," SIAM **22**, 602-616 (2000)

General Shiba mapping for on-site four-point correlation functions

Herbert Eßl, Matthias Reitner, Giorgio Sangiovanni & Alessandro Toschi

Shiba Transformation

Hubbard model with bipartite lattice

$$U \leftrightarrow -U$$
$$\delta\mu \leftrightarrow h$$
$$h \leftrightarrow \delta\mu$$

Connection between spin and density/gap function

$$\begin{matrix} S_x \\ S_y \\ S_z \end{matrix} \longleftrightarrow \begin{matrix} \mathrm{Re}(\Delta) \\ \mathrm{Im}(\Delta) \\ \rho \end{matrix}$$

Spin $SU(2)_S$ — Pseudospin $SU(2)_P$

What's new: Four-point Green's functions under Shiba mapping
Application to vertex divergences of Hubbard Atom

arXiv:2402.16115

Shift photoconductivity in the Haldane model

Shift current

- Light absorption process in homogeneous materials
- 2º order effect with $\vec{E}$

$$j^a = \sigma^{abc} E^b E^c$$

- Requires inversion symmetry breaking

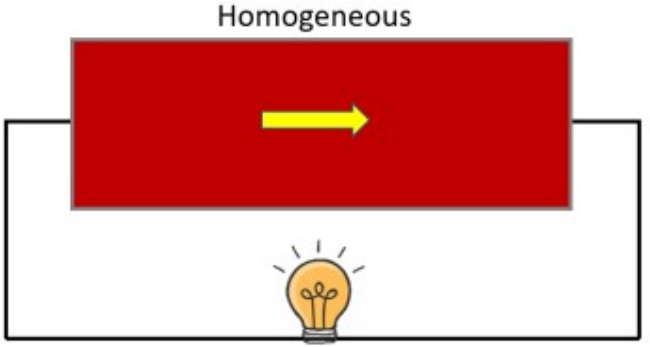

$$\sigma^{abc} = -\frac{i\pi e^3}{4\hbar^2} \int \frac{d\vec{k}}{(2\pi)^D} \sum_{mn} f_{nm} \left(r^b_{mn} r^{c;a}_{nm} + r^c_{mn} r^{b;a}_{nm} \right) \times \left[\delta\left(\omega_{nm} - \omega\right) + \delta\left(\omega_{mn} - \omega\right) \right].$$

Haldane model review

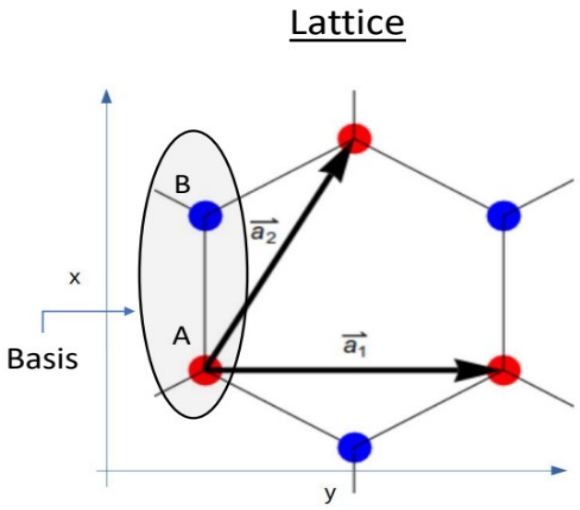

Tight-binding parameters

- Onsite energies $\pm M$ +(-) for A(B)
- nn tunnelings t_1
- nnn tunnelings $t_2 e^{i\pm\phi}$ +(-) for A(B)→ A(B)

Breaks IS

Breaks Time Reversal symmetry (TRS)

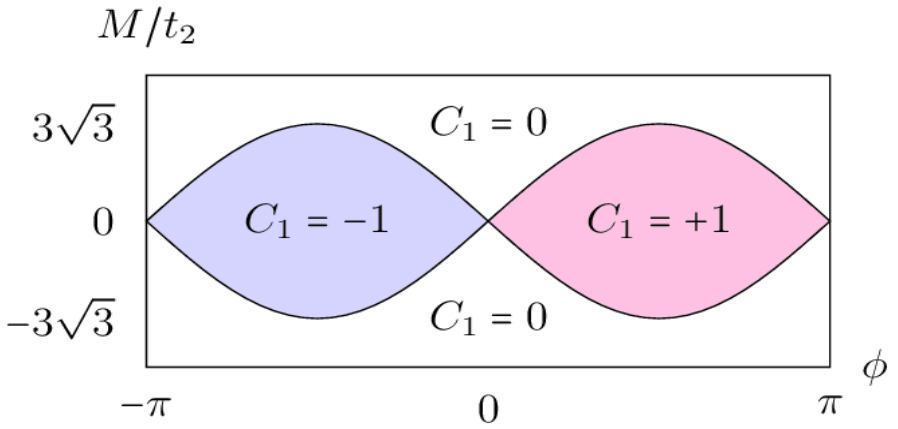

C_1: Chern number

Numerical evaluation: shift current

Deep tight-binding regime

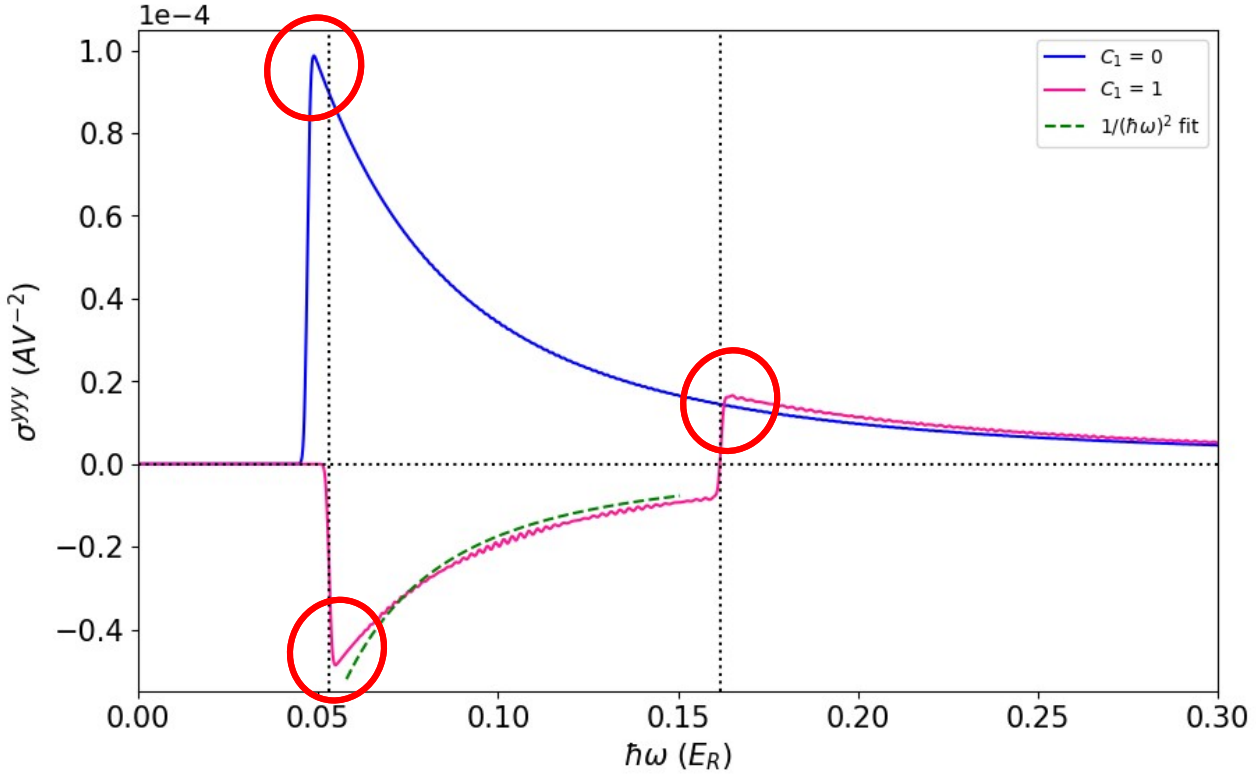

$$\sigma^{yyy}(\omega) = -\frac{e^3 a \,\mathrm{sign}\,[m(\chi)]}{(\hbar\omega)^2 |\eta\,(\chi)|}$$

Sign controlled by mass term

SU(N) dynamics of a phonon-driven spin-1 magnet

K. Hart, R. Sutcliffe, G. Refael, A. Paramekanti

1. SU(N) Monte Carlo and molecular dynamics WITH phonons

- SU(N) → dipole and quadrupole moments
- Phonons couple to quadrupoles linearly
- Driven-damped phonons

H_{sp} = strong single-ion anisotropy
H_{ph} = driven-damped oscillator
$H_{sp\text{-}ph}$ = quadrupoles × phonons

2. Out-of-equilibrium physics

- Two phonon drive = effective magnetic field

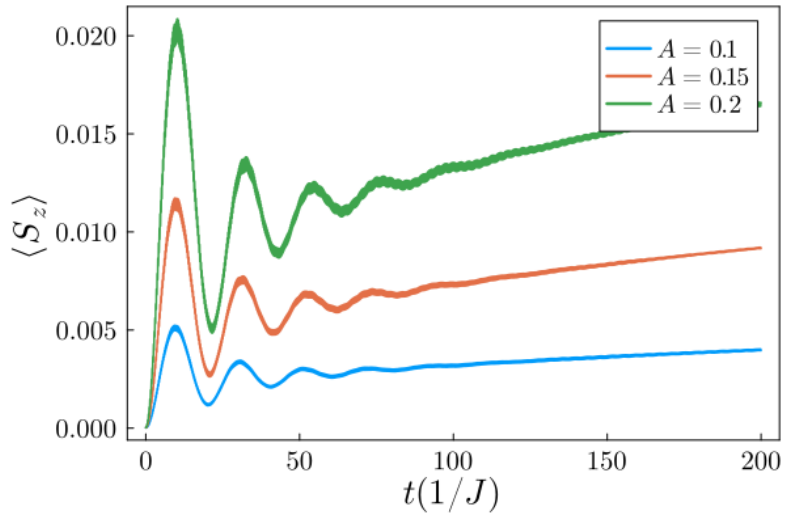

- One phonon drive = Floquet copies

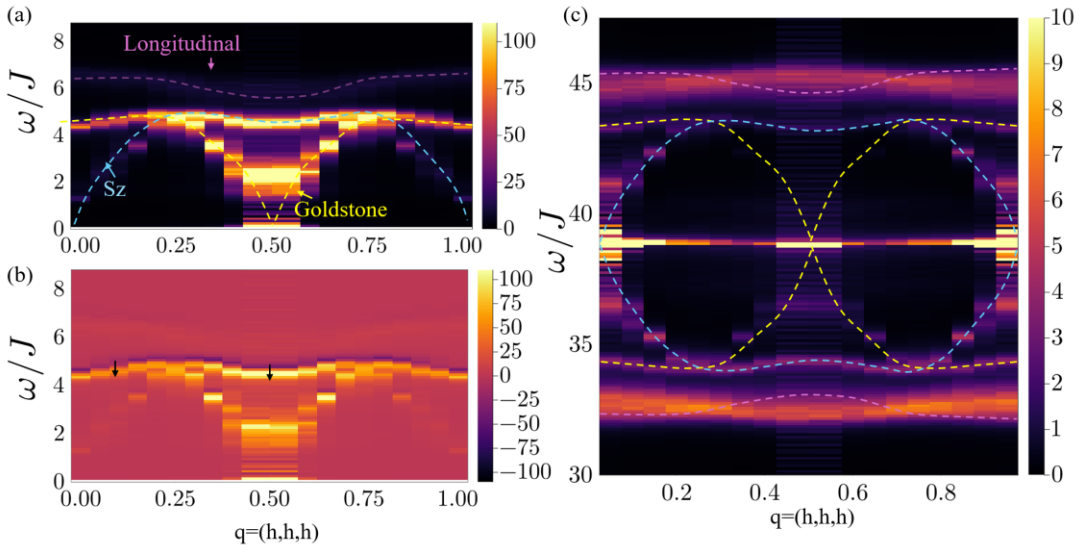

Superconductivity in a Hund Correlated Two Orbital Attractive Hubbard Model

L. Torchia M. Capone

MODEL

$$H_{int} = U \sum_{m} n_{m\uparrow} n_{m\downarrow} + (U-2J) \sum_{m \neq m'} n_{m\uparrow} n_{m'\downarrow} + (U-3J) \sum_{m<m',\sigma} n_{m\sigma} n_{m'\sigma}$$

Holstein coupling

$$U_{\text{eff.}} = U - \frac{2g^2}{\omega_0}$$

phonon-driven attraction

METHOD: DMFT + ED

RESULTS: comparison

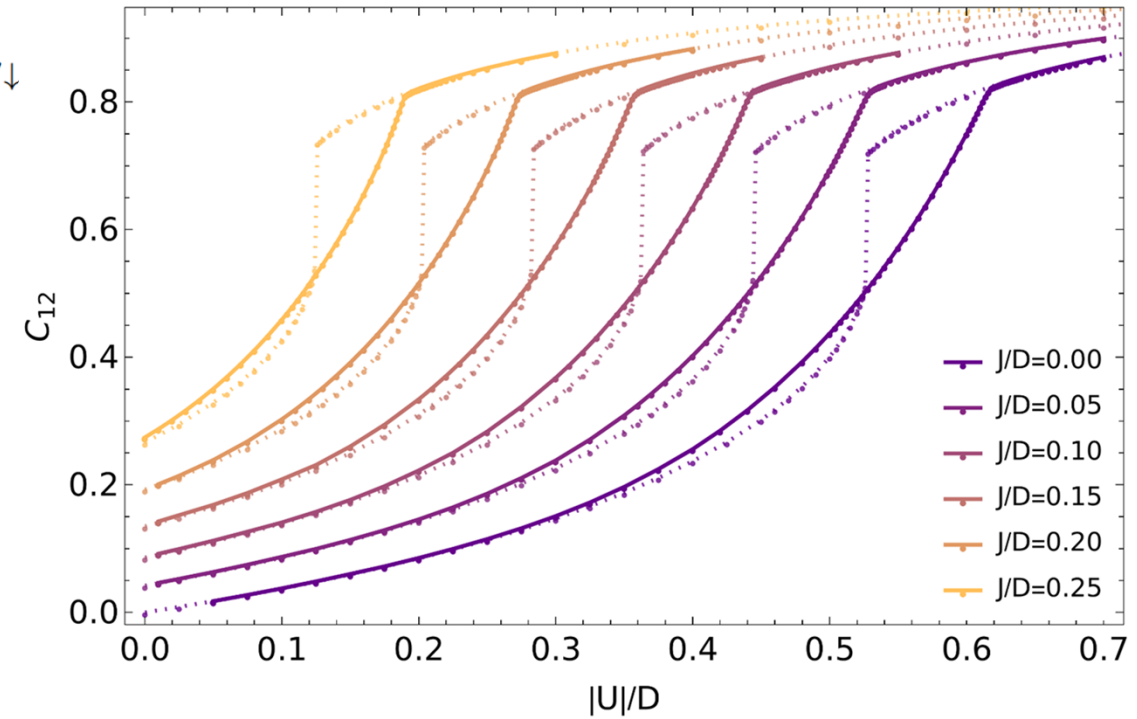

The pseudogap – Fermi liquid transition of the Hubbard model at arbitrary low temperatures

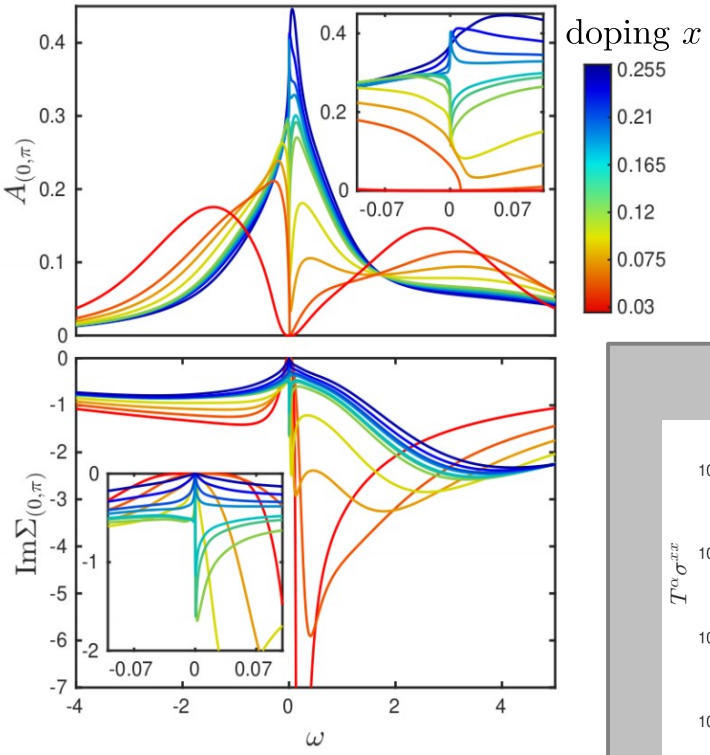

Fermi surface reconstruction at $x \approx 0.22$

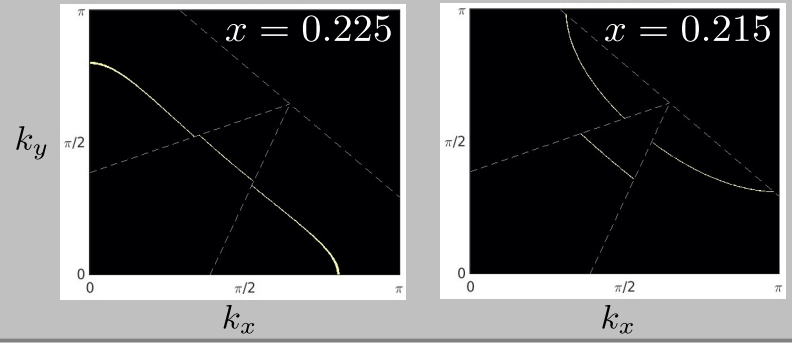

DCA+NRG

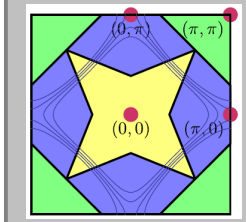

$t = 1$
$t' = -0.15$
$U = 7$
$T = 10^{-10}$

Optical contuctivity σ^{xx}

calculation experiment

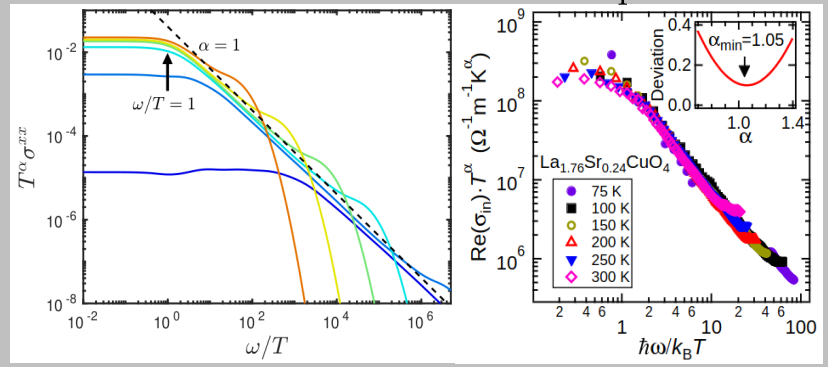

[X. Li *et al.*, Frontiers in Elec. Mat. 2, 2673-9895 (2023)]

Phasediagram

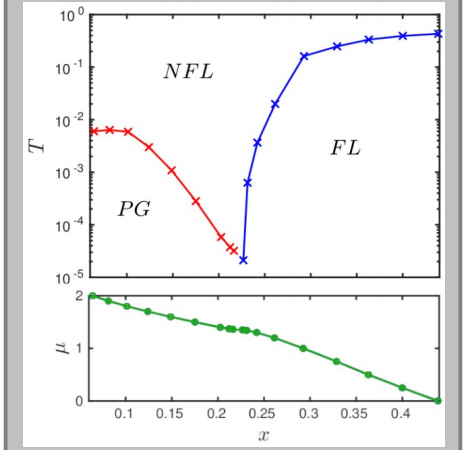

Mathias Pelz, Andreas Gleis, Seung-Sup Lee, Jan von Delft

Renormalized perturbation theory for fast evaluation of Feynman diagrams on the real frequency axis

M. D. Burke[1,2], Maxence Grandadam[1], and J. P. F. LeBlanc[1]

[1]*Department of Physics and Physical Oceanography, Memorial University of Newfoundland,* [2]*Department of Physics & Astronomy, University of Waterloo*

New numerical scheme evaluates Feynman Diagrams on the real frequency axis exponentially faster

What are Feynman Diagrams?

- Feynman Diagrams provide a pictorial representation for a series of interactions of particles in a many body system.
- A solid line is a fermion (e.g., electron) and a wavy line is boson (e.g., photon).
- Mathematically, these diagrams can be represented by an integral over all the internal degrees of freedom (momentum q, frequency $i\nu_1$) of the product of Green's functions for each fermion.

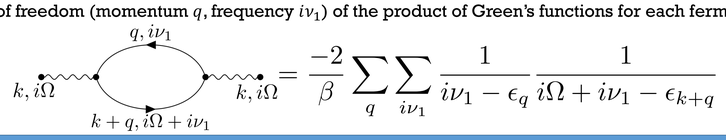

$$= \frac{-2}{\beta}\sum_{q}\sum_{i\nu_1}\frac{1}{i\nu_1-\epsilon_q}\frac{1}{i\Omega+i\nu_1-\epsilon_{k+q}}$$

Physical Model

- We use the single band Hubbard Model on 2D square lattice with nearest neighbour hopping, t, interaction, U, and $\mu = 0$.
- This restricts fermions to only reside at lattice sites and bosons are the interactions between sites.
- The fermions are allowed to hop to neighbouring sites.
- This corresponds to this Hamiltonian and particle dispersion,

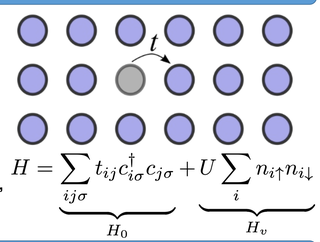

$$H = \underbrace{\sum_{ij\sigma} t_{ij} c^{\dagger}_{i\sigma} c_{j\sigma}}_{H_0} + \underbrace{U\sum_{i} n_{i\uparrow} n_{i\downarrow}}_{H_v}$$

$$\epsilon(\mathbf{k}) = -2t[\cos(k_x)+\cos(k_y)]$$

Algorithmic Matsubara Integration (AMI)

- Allows us to analytically evaluate frequency integrals encountered in the evaluation of Feynman Diagrams by using Cauchy's residue theorem. **[2]**
- Once an analytic expression is formed, we can then perform the analytic continuation that is required to evaluate on the real frequency axis

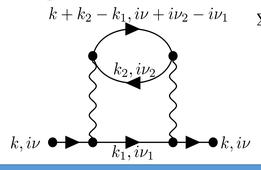

$$\Sigma^{(2)}(k,i\nu) = \frac{-U^2}{\beta^2}\sum_{\{k_i\}}\sum_{\{i\nu_n\}}\frac{1}{i\nu_1-\epsilon_{k_1}}\frac{1}{i\nu_2-\epsilon_{k_2}}\frac{1}{i\nu+i\nu_2-i\nu_1-\epsilon_{k+k_2-k_1}}$$

(AMI)

$$= \sum_{\{k_i\}}\frac{-U^2(f(\epsilon_{k_1})-f(\epsilon_{-k}))(f(\epsilon_{k_2})+n(\epsilon_{k_1+k}))}{i\nu+\epsilon_{k_2}-\epsilon_{k_1}-\epsilon_k}$$

Analytic continuation

$$i\nu \to \omega + i\Gamma, \Gamma \to 0^+$$

Real Frequency Issues - Analytic Continuation

- We must perform an analytic continuation to the expression returned from AMI. However, this is a problem as the integrand has peaks with widths proportional to Γ.
- This leads to insufficient sampling of integrand in Monte Carlo methods to evaluate the remaining momentum integrals.

$$G_0^{-1}(k,\omega,\Gamma) = \omega - \epsilon_k + \mu + i\Gamma\,, \Gamma \to 0^+$$

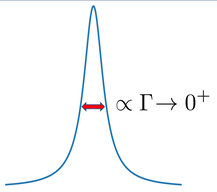

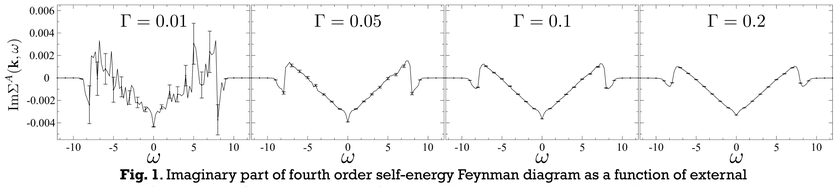

Fig. 1. Imaginary part of fourth order self-energy Feynman diagram as a function of external real frequency, ω, for various values of the analytic continuation parameter, Γ.

- In **Fig. 1**, we see that taking a value of Γ too small (0.01), we get a large uncertainty in the integration. Also, by taking a larger value of Γ the error goes down, but the graphs lose sharp features at $\omega = 0$ and $\omega = \pm 7.5$, which is not physically correct!
- Our method addresses this issue which leads to exponentially faster calculations with small Γ.

Renormalized Perturbation Theory

- Like all perturbative methods, we start with a problem that we know the answer to, but then make slight corrections to get an approximate answer to another problem that would otherwise be difficult to solve.
- We introduce a single particle term δ and insert it into our Hamiltonian while leaving it unchanged:

$$\delta = z\sum_{i\sigma}\hat{n}_{i\sigma}, \exists z \in \mathbb{C}$$

$$\begin{aligned} H &= H_0 + H_v + \delta - \delta \\ &= (H_0 - \delta) + (H_v + \delta) \\ &= H_0' + H_v'. \end{aligned}$$

- Expanding about the known solution of H_0' with respect to H_v' we have:

$$G_0^{-1}(k, i\omega_n) = i\omega_n - \epsilon_k + \mu + z$$

- The expansion of H_v' in comparison to H_v spawns an infinite set of counter-term diagrams with self-energy insertions, shown in **Fig. 2**.

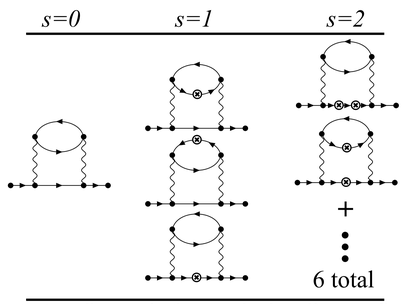

Fig. 2. Counter-term diagrams for the second order self-energy diagram. Here s denotes the number of insertions that are placed on the root diagram. This leads a to a combinatorically growing number of diagrams for each value of s.

- Thus, any diagram that we were going to include in our calculations is then replaced by an infinite series of diagrams.

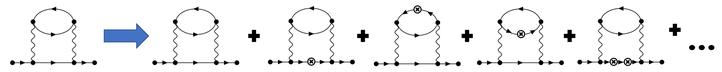

- The benefit of this method is seen by taking a purely imaginary value of $z = i\alpha$

$$G_0^{-1}(k, i\omega_n) = i\omega_n - \epsilon_k + \mu + z \quad i\omega_n \to \omega + i\Gamma$$

$$G_0^{-1}(k,\omega,\Gamma) = \omega - \epsilon_k + \mu + i(\Gamma + \alpha)$$

- By choosing $z = i\alpha$ with $\alpha \gg \Gamma$, we find that the widths of previously troubling peaks now are proportional to $\alpha + \Gamma$ so we can take $\Gamma \to 0^+$.

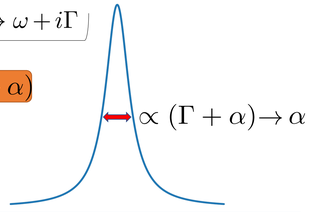

Recap of the Method - *"There is no free lunch"*

- We modify our functions so that they are easy to integrate at the cost of summing an infinite series of diagrams. Luckily, the infinite series has the form:

$$\Sigma_k(i\omega_n) = \sum_{\ell=0}^{\infty}\sum_{s=0}^{\infty} a_{\ell,s}(z)U^{\ell}(z)^s \quad \Rightarrow \quad \Sigma_k^{(m,c)}(i\omega_n, z) = \sum_{\ell=0}^{m}\sum_{s=0}^{c} a_{\ell,s}(z)U^{\ell}(z)^s$$

- That is, each term with s insertions is weighted by z^s. Meaning for a choice of z so that $|z| \ll R$, where R is the radius of convergence of the untruncated series ($R = i\omega_0$) **[3]**, the higher order terms become negligible.
- So, we truncate the series to m^{th} order diagrams with c number of insertions as shown.

Results

- We first compare the results of our new method with the old method in **Fig. 3**.
- Right pane is our proposed approach, left pane is the original way of evaluating the diagrams.
- Note that various choices of z with 2 insertions approaches the same value and using 3 insertions brings the values even closer.

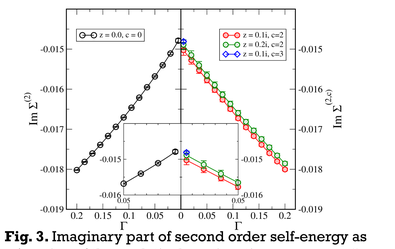

Fig. 3. Imaginary part of second order self-energy as a function of the analytical continuation parameter, Γ.

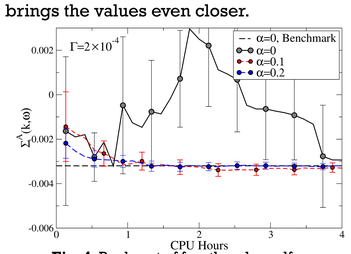

Fig. 4. Real part of fourth order self-energy diagram as a function of the computational time for various methods.

- In **Fig. 4**, a fourth order diagram is plotted as a function of computational time with $\Gamma = 2\times10^{-4}$.
- The benchmark data was acquired using the old method and took 640 CPU hours to converge. In contrast to our Renormalized PT approach which converged to the correct answer in about 5 hours.
- This is an improvement of about 120 times as fast.

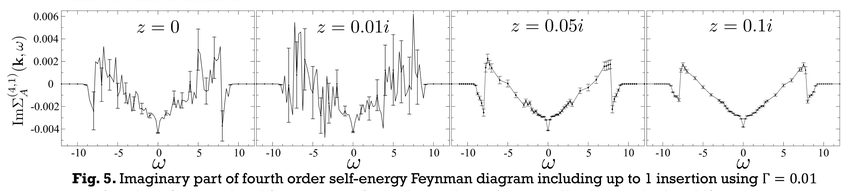

Fig. 5. Imaginary part of fourth order self-energy Feynman diagram including up to 1 insertion using $\Gamma = 0.01$ as a function of external real frequency, ω, for various values of renormalized perturbative shifts, z.

- **Fig. 5** shows the effect of taking different values of z. For a large enough α (> 0.01), we see preserved features that are lost in **Fig. 1**.
- **Fig. 6** shows a physical application of our new approach using $\Gamma = 10^{-3}$ to obtain the density of states of a material.
- This displays the physically correct metal insulator transition from $U = 3 \to 4$ for the value of $\beta = 5$.
- This expansion included a total of 143 diagrams, but due to the added numerical broadening these diagrams are now easier to evaluate.

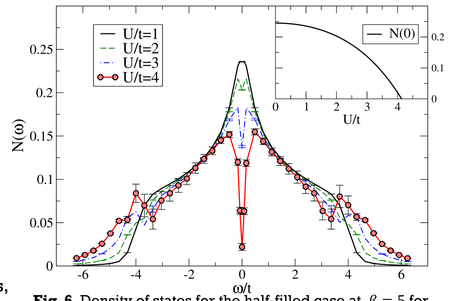

Fig. 6. Density of states for the half-filled case at $\beta = 5$ for $\Gamma = 0.001$. Here we use $z = 0.2i$ truncated at 1 insertion for fourth order diagrams and 2 insertions at other orders.

Conclusions

- We introduced a new method to evaluate Feynman diagrams on the real frequency axis.
- This method creates a new numerical regulator whose effect is removed by including several easier-to-evaluate diagrams. This regulator broadens peaks in integrands so that they can be evaluated via a Monte Carlo integration scheme exponentially faster.
- This method has a potentially massive advantage if a fine-tuned choice of z is used so that a limited number of extra diagrams need to be summed.

References

[1] Burke, M.D. *et al,* Phys. Rev. B **107**, 115151 (2023)
[2] Taheridehkordi, A. *et al,* Phys. Rev. B **99**, 035120 (2019)
[3] Vučičević, J. *et al,* Phys. Rev. Research **3**, 023082 (2021)

Acknowledgments

This work was made possible by various NSERC grants and computational resources provided by the Digital Research Alliance of Canada/Compute Canada.

Scan for the full paper!

MEMORIAL UNIVERSITY · UNIVERSITY OF WATERLOO · NSERC CRSNG · Digital Research Alliance of Canada | Alliance de recherche numérique du Canada · compute canada | calcul canada

Phonon-driven detection and control of multipolar order in d^2 Mott insulators

- Pseudospin-1/2 model of Osmate double perovskites coupled to E_g phonons

1) Pump-probe spectroscopy
   - Energy transfer between phonons
2) Non-equilibrium steady states
   - Effective magnetic field

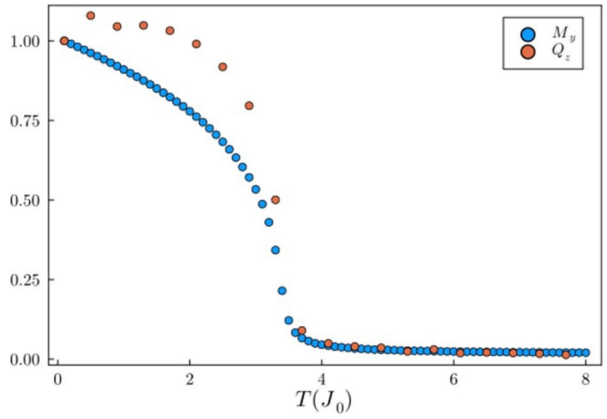

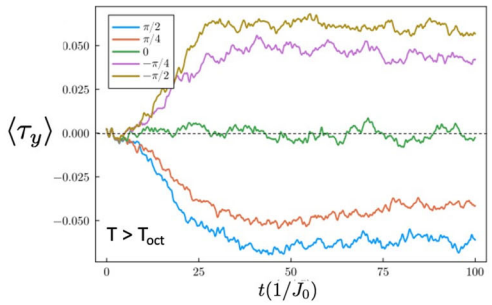

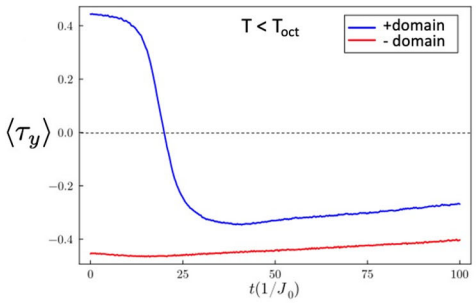

Altermagnetism and superconductivity in multiorbital t-J model

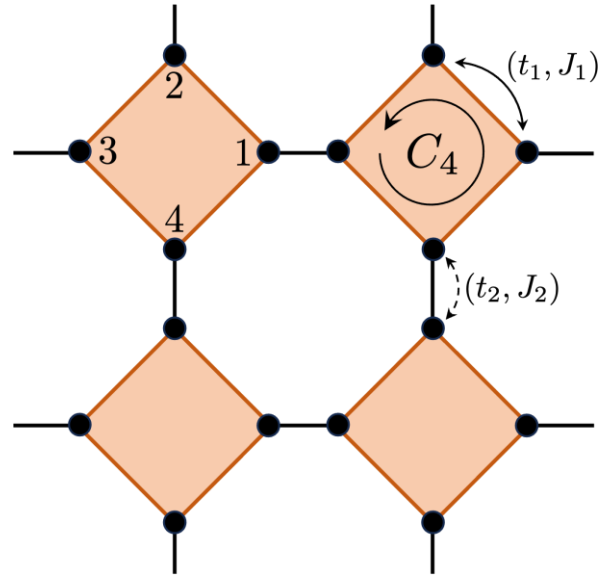

Study of magnetic and pairing instabilities driven by exchange interactions:

- Hartree-Fock-Bogoliubov theory treatment of multiorbital model

Rich phase diagram:

- D-wave/s-wave superconductor
- ALM/AFM magnetic ordering

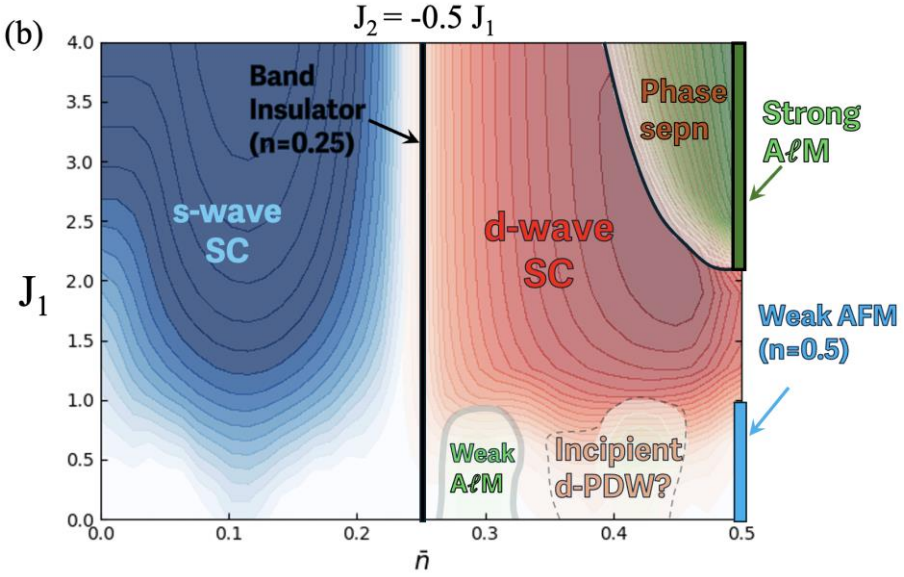

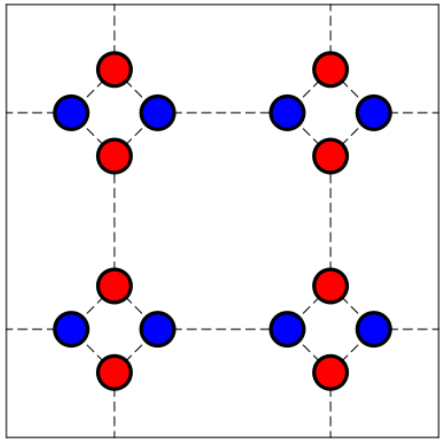

Seebeck coefficient in the repulsive Fermi Hubbard model

S. Roy, A. Samanta, N. Trivedi

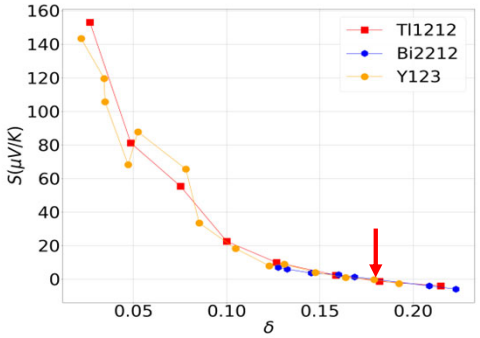

Universal signatures of Seebeck coefficient in cuprates:

- Anomalous sign change at finite doping.
- Divergence near half filling.

Interaction/charge gap driven?

Parent hamiltonian of cuprates – Repulsive Fermi Hubbard model

$$H = -\sum_{\langle i,j\rangle,\sigma}(t_{ij}\hat{c}^{\dagger}_{i,\sigma}\hat{c}_{j,\sigma} + \text{h.c}) - \mu\sum_{i,\sigma}\hat{n}_{i,\sigma} + U\sum_{i,\sigma}(\hat{n}_{i,\uparrow} - \frac{1}{2})(\hat{n}_{i,\downarrow} - \frac{1}{2})$$

nearest neighbor hopping — sets doping — particle hole symmetric

Investigate by Kelvin formula for thermopower

$$S_{\text{Kelvin}} = \lim_{q_x\to 0,\omega\to 0} S_{\text{Kubo}}(q_x,\omega) \quad = -\frac{1}{e}\frac{\partial\mu}{\partial T}\Big|_{V,n} = \frac{1}{e}\frac{\partial s}{\partial n}\Big|_{T,V}$$

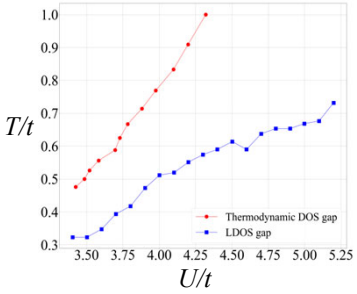

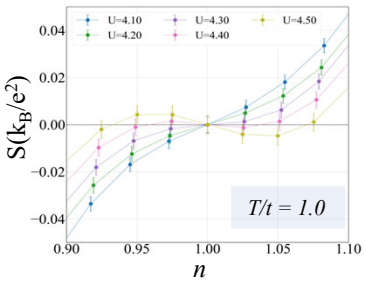

Approach to free particle of Seebeck coefficient limit through many body gap closing

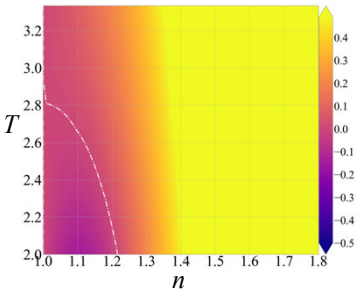

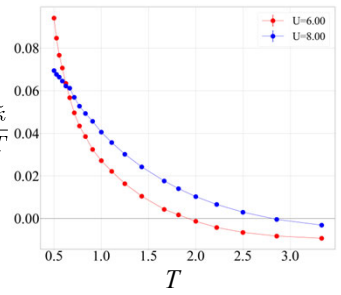

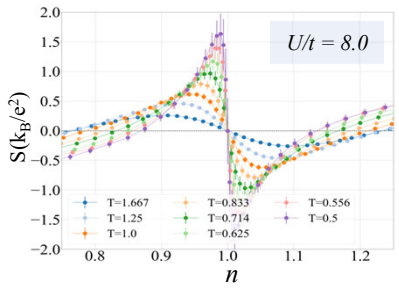

Local moment formation and Seebeck anomaly:

- Anomalous Seebeck coefficient in concurrence with local moment formation.
- Divergence of Seebeck is due to singlet formation between neighboring sites.
- Approach to free particle limit is nonmonotonic wrt temperature.

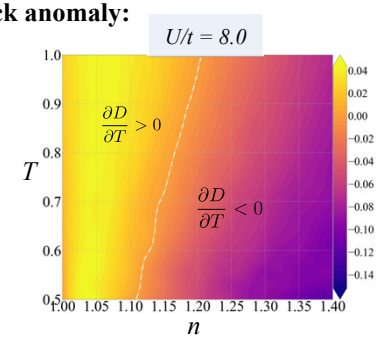

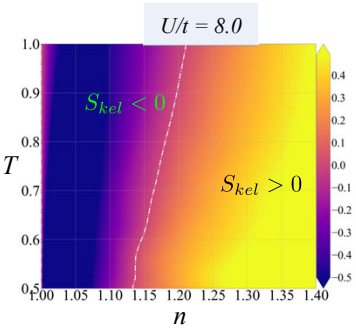

Parton construction: Effective low energy hamiltonian – *t-J* model:

$$H_{eff} = -t\sum_{\langle ij\rangle,\sigma}\hat{c}^{\dagger}_{i\sigma}\hat{c}_{j\sigma} + J\sum_{\langle ij\rangle}[\vec{S}^i\cdot\vec{S}^j - \frac{1}{4}n_in_j]$$

$$\hat{c}^{\dagger}_{i\sigma} = \hat{f}^{\dagger}_{i\sigma}\hat{h}_i + \sigma\hat{f}_{i\bar{\sigma}}\hat{d}^{\dagger}_i \qquad \hat{d}^{\dagger}_i\hat{d}_i + \hat{h}^{\dagger}_i\hat{h}_i + \sum_{\sigma}\hat{f}^{\dagger}_{i,\sigma}\hat{f}_{i\sigma} = 1$$
$$\hat{c}_{i\sigma} = \hat{h}^{\dagger}_i\hat{f}_{i\sigma} + \sigma\hat{d}_i\hat{f}^{\dagger}_{i\bar{\sigma}} \qquad \hat{c}^{\dagger}_{i\sigma}\hat{c}_{i\sigma} = \hat{d}^{\dagger}_i\hat{d}_i + \hat{f}^{\dagger}_{i\sigma}\hat{f}_{i\sigma}$$

- Only keep order parameters associated with charge degrees of freedom.
- Sufficient to capture Seebeck anomaly.

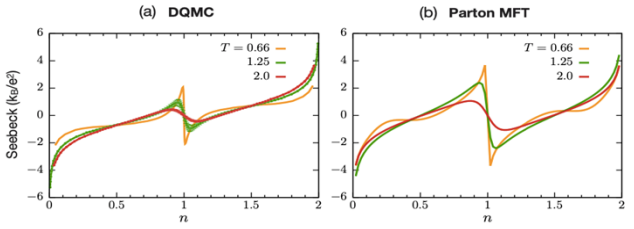

Two-particle calculations with QTCI

Iteratively solving the parquet equations

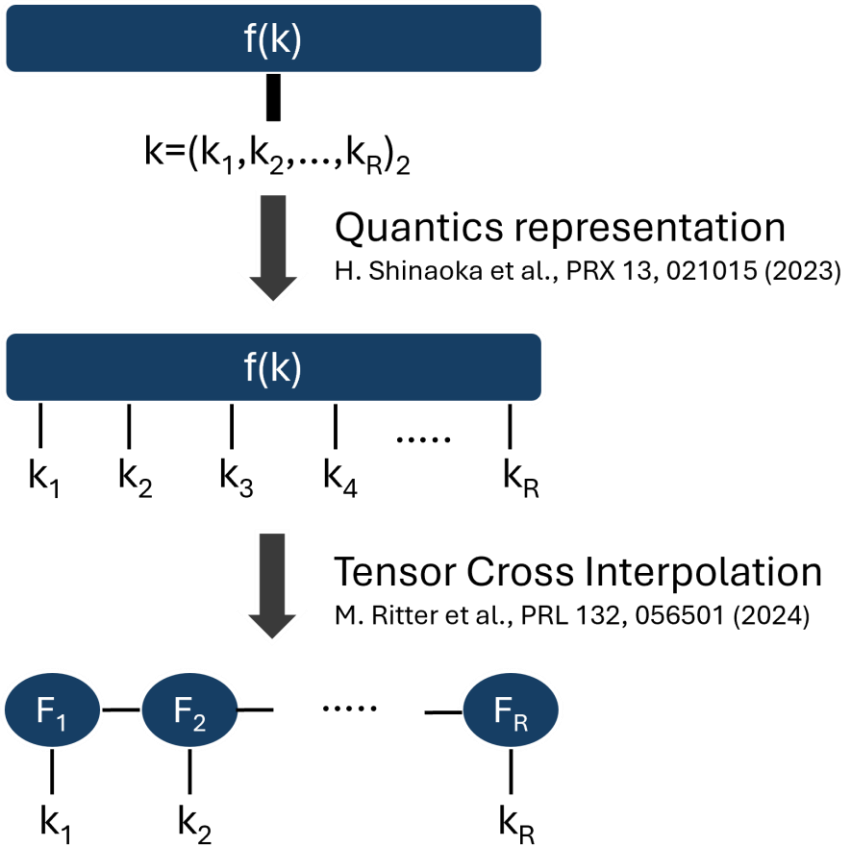

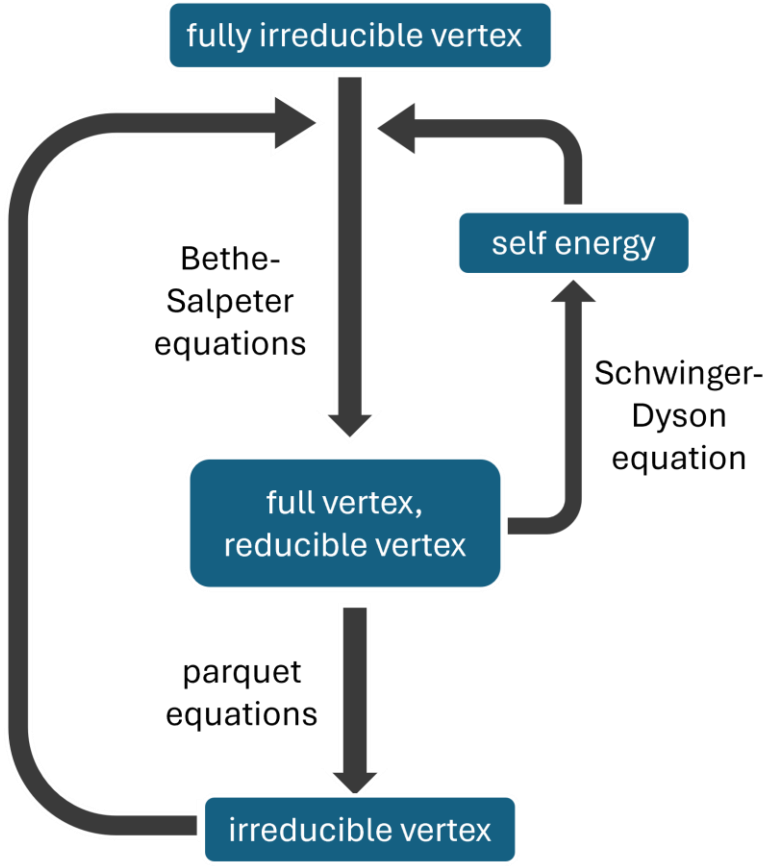

Stefan Rohshap, Marc Ritter, Hiroshi Shinaoka, Markus Wallerberger, and Anna Kauch
Computational Quantum Materials School 2024

TECHNISCHE UNIVERSITÄT WIEN
Vienna | Austria

Unveiling Frustrated Interactions in $BaCo_2(AsO_4)_2$ with the Magnetotropic Susceptibility

Poster by: William Bateman-Hemphill
Publication by: Shiva Safari, William Bateman-Hemphill, Asimpunya Mitra, Félix Desrochers, Emily Z. Zhang, Lubuna Shafeek, Austin Ferrenti, Tyrel M. McQueen, Arkady Shekhter, Zoltán Köllö, Yong Baek Kim, B. J. Ramshaw, K. A. Modic

UNIVERSITY OF TORONTO

Main Conclusion

- $BaCo_2(AsO_4)_2$ (often called BCAO) was first thought of as a quantum spin liquid candidate, is now known to be **magnetically ordered**
- One might still hope to induce a QSL using out-of-plane magnetic field
- In this work, we map the field-induced phase diagram of BCAO and determine that it can be mostly explained by a classical model with long-range ordered states

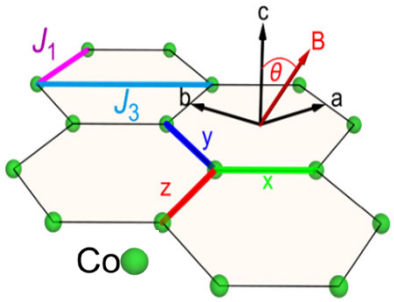

Field-Induced Phase Diagram

- Monte Carlo Calculations (pink) reproduce the qualitative features of the magnetotropic susceptibility (A) and the shape of the phase diagram (B)

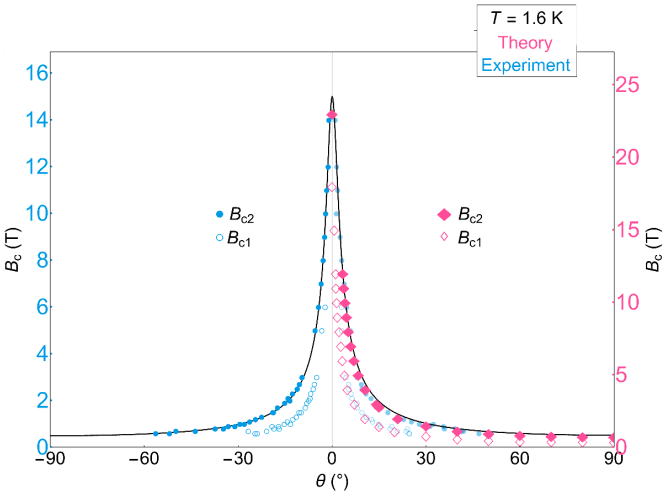

- Excellent qualitative agreement with experiment!
- All critical fields are over-estimated by a factor ~1.6

Quantum Phase Diagram from iDMRG

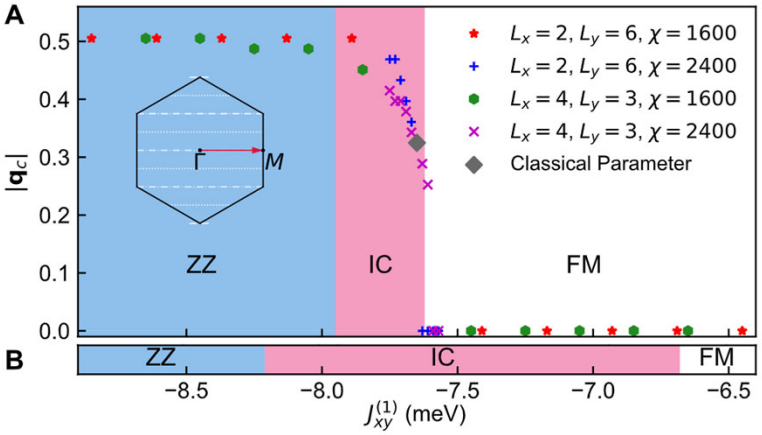

Conclusion

- $BaCo_2(AsO_4)_2$ is well-described by a classical model as an easy-plane magnet
- Quantum fluctuations likely play a role in suppressing the critical fields significantly

To be, or not to be, phonon-mediated ?

Jean-Baptiste de Vaulx - Institut Néel, CNRS, Grenoble, France

Nickelates : new family of superconductors.

Show strong analogies with the cuprates.

But are nickelates conventional superconductors ?

Our work (Meier et al. Phys. Rev. B 109 (18): 184505) **:**

- G_0W_0@DFT electronic structures calculations
- Electron-phonon coupling calculations within Eliashberg theory

Results :

- Analysis of doping and pressure behavior in comparison with experiment confirms the non-phonon mediated nature of nickelates.
- **Superconductivity mechanism remains unconventional !**

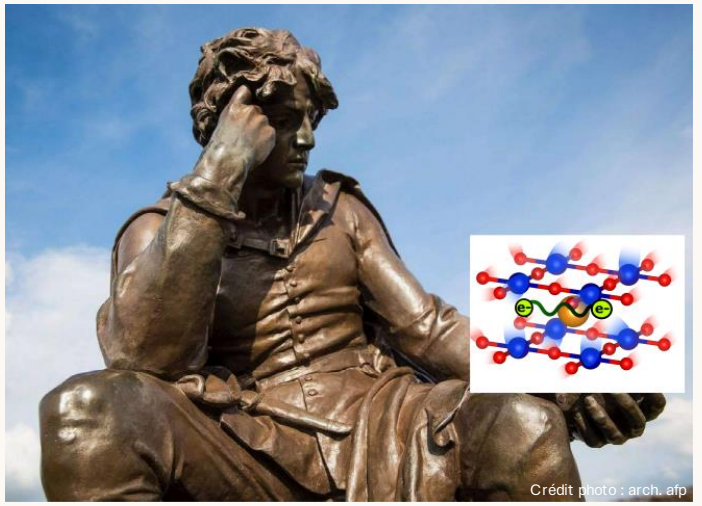

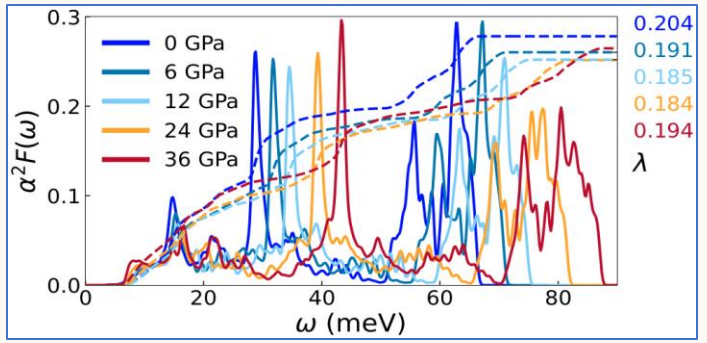

And moreover : Correlation-induced self-doping and Lifshitz transition in La_2NiO_4